Resource-Theoretical Unification of Mpemba Effects: Classical and Quantum

Alessandro Summer,[1,2,*] Mattia Moroder,[1,2,†] Laetitia P. Bettmann,[1,‡] Xhek Turkeshi,[3,§] Iman Marvian,[4,5,‖] and John Goold[1,2,¶]

[1]*School of Physics, Trinity College Dublin, Dublin 2, Ireland*
[2]*Trinity Quantum Alliance, Unit 16, Trinity Technology and Enterprise Centre, Pearse Street, D02 YN67, Dublin 2, Ireland*
[3]*Institut für Theoretische Physik, Universität zu Köln, Zülpicher Strasse 77, 50937 Köln, Germany*
[4]*Duke Quantum Center and Department of Physics, Duke University, Durham, North Carolina 27708, USA*
[5]*Department of Electrical and Computer Engineering, Duke University, Durham, North Carolina 27708, USA*

(Received 1 August 2025; revised 20 November 2025; accepted 6 January 2026; published 25 March 2026)

The Mpemba effect originally referred to the observation that, under certain thermalizing dynamics, initially hotter samples can cool faster than colder ones. This effect has since been generalized to other anomalous relaxation behaviors even beyond classical domains, such as symmetry restoration in quantum systems. This work demonstrates that resource theories, widely employed in information theory, provide a unified organizing principle to frame Mpemba physics. We show how the conventional thermal Mpemba effect arises naturally from the resource theory of athermality, while its symmetry-restoring counterpart is fully captured by the resource theories of asymmetry. Leveraging the framework of modes of asymmetry, we demonstrate that the Mpemba effect due to symmetry restoration is governed by the initial overlap with the slowest symmetry-restoring mode, mirroring the role of the slowest Liouvillian eigenmode in thermal Mpemba dynamics. Through this resource-theoretical formalism, we uncover the connection between these seemingly disparate effects and show that the dynamics of thermalization naturally splits into a symmetry-respecting and a symmetry-breaking term.

DOI: 10.1103/rbt4-psfd

Subject Areas: Complex Systems, Quantum Physics, Statistical Physics

I. INTRODUCTION

The Mpemba effect originally described the anomalous situation of a hot system cooling down faster than a warm one. First investigated by Mpemba and Osborne in water in 1969 [1], it has since then been observed in various physical systems ranging from clathrate hydrates [2] to crystallization processes in polymers [3] and magnetic transitions in alloys [4]. Following its precise mathematical characterization in classical systems coupled to Markovian environments [5], the effect was further investigated theoretically [6–9] and experimentally [10–12] for colloidal systems. Two further important directions in the study of the classical Mpemba effect concern driven granular gases [9,13,14] and phase transitions [15,16]. The latter, despite pertaining to the phenomenon as originally observed in water, remains the most challenging and least understood case [17,18].

In recent years, the theoretical framework was extended to quantum systems [19–31]. In this context, a related phenomenon has been observed in the dynamical restoration of symmetries: States that initially display stronger symmetry breaking can *locally* [32] restore it faster than states with initially weaker symmetry breaking [33,34]. We refer to this phenomenon as the *symmetry* Mpemba effect, to differentiate it from the conventional *thermal* Mpemba effect pertaining to thermalization dynamics.

In this article, we establish a framework to understand both the thermal and symmetry Mpemba effects on the same footing using resource theories (RTs) [35,36], which are widely used in quantum information theory. A Mpemba effect arises when two resourceful states evolve under the same dynamics, and the more resourceful one dissipates the resource faster than the less resourceful one, causing their

*Contact author: summera@tcd.ie
†Contact author: moroderm@tcd.ie
‡Contact author: bettmanl@tcd.ie
§Contact author: turkeshi@thp.uni-koeln.de
‖Contact author: iman.marvian@duke.edu
¶Contact author: gooldj@tcd.ie

Published by the American Physical Society under the terms of the Creative Commons Attribution 4.0 International license. Further distribution of this work must maintain attribution to the author(s) and the published article's title, journal citation, and DOI.

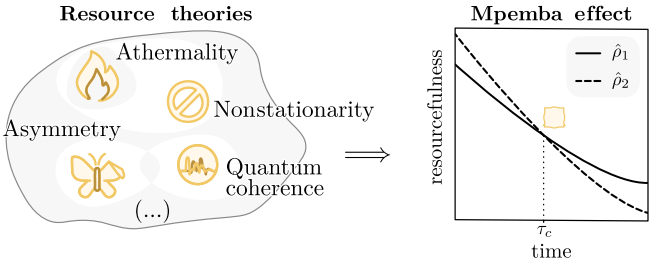

FIG. 1. In a resource-theoretic framework, the Mpemba effect occurs when a state that initially possesses more of a given resource depletes that resource faster than a less resourceful state, under the evolution by the same free operation, so that their resource monotones cross. This single picture unifies a variety of anomalous equilibration phenomena (for example, restoring thermal equilibrium or symmetry in classical and quantum systems). Mpemba physics then becomes the study of why different initial states dissipate resources at different rates and how we can harness those differences to engineer exotic effects such as ultrafast cooling. In this article, we apply this analysis to the specific resource theories shown in the schematic.

resource monotones to cross. This description allows us to capture the essence of both effects within a single conceptual framework (see Fig. 1). Building upon this, we employ the framework of modes of asymmetry [37] to explain the occurrence of the symmetry Mpemba effect. Analogous to how the thermal Mpemba effect is understood in terms of overlaps with slow relaxation modes [5], we demonstrate that the symmetry Mpemba effect also arises when strongly symmetry-broken initial states have small (or vanishing) overlap with the slowest symmetry-restoring mode. Within this framework, we study various examples revealing that the thermal Mpemba effect can also occur in subsystems of unitarily evolving systems, while the symmetry Mpemba effect can manifest in quantum systems under Lindblad evolution and in purely classical Markovian dynamics, as well as circuits with Abelian (continuous) and non-Abelian symmetries. In this context, we emphasize that the specific type of Mpemba effect observed is dictated by the chosen measure for quantifying the relaxation process rather than being an intrinsic property of the physical system itself. Finally, in the presence of arbitrary symmetries, we highlight the connection between the nonequilibrium free energy, commonly used for the thermal Mpemba effect, and the relative entropy of asymmetry (also known as entanglement asymmetry), a measure for the asymmetry of a state.

To guide the reader through the paper, Mpemba effects originated from different RT are indicated via different symbols: □ for athermality, ○ for asymmetry, △ for symmetry-respecting athermality, and ☆ for nonstationarity.

This article is organized as follows: First, in Sec. I A, we concisely present some basic concepts regarding RTs. Subsequently, in Sec. II, we explore the occurrence of the thermal Mpemba effect in various classical and quantum setups from the perspective of RTs. Then, we introduce the modes of asymmetry in Sec. III and employ them to identify fast-equilibrating states in the context of the symmetry Mpemba effect. In Sec. IV, we provide a unified description of the thermal and the symmetry Mpemba effect, and, finally, in Sec. V, we summarize our findings and point toward future applications.

A. Resource theories

Resource theories (RTs) (see Ref. [36] for a review) provide the natural language for understanding and unifying diverse Mpemba effects: They formalize which state transformations are possible when only certain *free* operations are allowed and, thereby, translate relaxation processes into the decay of a resource monotone [38]. In a nutshell, a resource theory is defined by two foundational ingredients: a set of free states and a class of free operations. Free operations are completely positive and trace-preserving (CPTP) maps that are considered accessible at no cost, either because they are physically implementable with minimal resources or because they reflect fundamental constraints of the theory. Similarly, the set of free states, denoted $\mathscr{F} \subset \mathscr{S}(\mathscr{H}_s)$ [where $\mathscr{S}(\mathscr{H}_s)$ indicates the set of density operators on the Hilbert space $\mathscr{H}_s$], consists of states that can be prepared at no cost. A minimal requirement that any resource theory must satisfy is that the set of free states is closed under free operations (as defined later in this section); that is, for any free state $\hat{\pi} \in \mathscr{F}$ and any free operation $\mathcal{E}$, we have $\mathcal{E}[\hat{\pi}] \in \mathscr{F}$. This closure condition ensures that no resource can be generated from within the free set. All states outside the free set, i.e., $\mathscr{S}(\mathscr{H}_s)\backslash\mathscr{F}$ [39], are called resourceful or nonfree. These are states that cannot be obtained from any free state using only free operations. Their preparation requires access to nonfree operations, and they are typically the carriers of some operational advantage within the theory. The presence and quantification of such states lie at the core of resource-theoretic approaches.

To familiarize with these concepts, we recall two prominent examples of quantum resource theories: the firstly defined one, bipartite entanglement, and classical ones, athermality in classical systems. In the theory of bipartite entanglement, the free states are separable states, and the free operations are local operations and classical communication (LOCC) [40]. Entangled states lie outside the free set and enable tasks such as quantum teleportation or the violation of Bell inequalities, which are impossible under LOCC alone. A fully classical example is provided by the RT of athermality for classical systems. Here, one considers a system in contact with a thermal environment at inverse temperature β. The free operations, also called thermal operations (TOs), are stochastic maps with fixed point given by the Gibbs distribution $(\boldsymbol{\pi}_\beta)_i \propto e^{-\beta E_i}$, which is also the only free state [41]. Any state that departs from

$\boldsymbol{\pi}_\beta$, therefore, possesses athermality, representing a source of nonequilibrium free energy that can be harnessed to perform useful work or drive transformations that are otherwise forbidden under thermal operations. We analyze this theory more in depth in Sec. II A, seeing how it naturally extends to quantum systems, too.

A resource monotone is a function $M:\mathscr{S}(\mathscr{H}_s)\to[0,\infty)$ satisfying two key properties

(1) vanishing for free states: $\hat{\rho}\in\mathscr{F}\Rightarrow M(\hat{\rho})=0$ and
(2) monotonicity under free operations: For every state $\hat{\rho}$ and every $\mathcal{E}\in\mathscr{O}$,

$$M(\mathcal{E}[\hat{\rho}])\le M(\hat{\rho}), \tag{1}$$

where $\mathscr{O}$ is the set of free operations.

A Mpemba effect manifests when two initial states $\hat{\rho}_1$ and $\hat{\rho}_2$ satisfying $M(\hat{\rho}_1)>M(\hat{\rho}_2)$ evolve under the same free operation $\mathcal{E}_t$ so that

$$M(\mathcal{E}_t[\hat{\rho}_1])<M(\mathcal{E}_t[\hat{\rho}_2]) \qquad \text{for some } t>0, \tag{2}$$

indicating that the more resourceful state has dissipated the resource faster.

To quantify resourcefulness, we adopt the family of Petz-Rényi α divergences [42]

$$M_\alpha(\hat{\rho})=\min_{\hat{\pi}\in\mathscr{F}} S_\alpha(\hat{\rho}\|\hat{\pi}), \qquad \alpha\in(0,1)\cup(1,2], \tag{3}$$

where

$$S_\alpha(\hat{\rho}\|\hat{\pi})=\frac{1}{\alpha-1}\ln \mathrm{Tr}[\hat{\rho}^\alpha\hat{\pi}^{1-\alpha}] \tag{4}$$

obeys the data-processing inequality under any CPTP map [36,42] and recovers the quantum relative entropy of resource for $\alpha\to 1$, i.e.,

$$M(\hat{\rho})=\min_{\hat{\pi}\in\mathscr{F}} S(\hat{\rho}\|\hat{\pi}), \tag{5}$$

where $S(\hat{\rho}\|\hat{\pi})=\mathrm{Tr}[\hat{\rho}(\ln\hat{\rho}-\ln\hat{\pi})]$ is the quantum relative entropy, i.e., the quantum generalization of the Kullback-Leibler (KL) divergence. Physically, M_α measures the divergence of $\hat{\rho}$ with respect to the closest free state in the Rényi sense. We note that Eqs. (3) and (5) follow the standard entropic and divergence route to construct monotones in general resource theories (vanish on the free states and nonincreasing under the free operations; see Ref. [43]).

II. THE THERMAL MPEMBA EFFECT

The first rigorous mathematical description of the thermal Mpemba effect was given in 2017 by Lu and Raz, who studied discrete-state continuous-time Markovian processes. In Ref. [5], the dynamics is generated by a classical Liouvillian $\hat{\mathcal{L}}^{\mathrm{cl}}$, whose eigenvalues λ_k are nonpositive, and it is convenient to order them in decreasing order of their real part as $0=\lambda_1>\mathrm{Re}(\lambda_2)\ge\mathrm{Re}(\lambda_3)\ge\cdots$. The classical Liouville equation (see Sec. II B) dictates that the contribution to the dynamics from all eigenmodes $\mathbf{r}_k$ of $\hat{\mathcal{L}}^{\mathrm{cl}}$ decay exponentially in time with a rate given by the real part of the corresponding eigenvalue, except for $\mathbf{r}_1$ corresponding to $\lambda_1=0$ that describes the thermal steady state. Thus, at long times, the equilibration speed of typical states will be proportional to $\exp[\mathrm{Re}(\lambda_2)t]$. Instead, special initial states having zero overlap with the so-called slowest-decaying mode $\mathbf{r}_2$ will equilibrate exponentially faster, with speed $\propto\exp[\mathrm{Re}(\lambda_3)t]$, provided that $\mathrm{Re}(\lambda_3)\neq\mathrm{Re}(\lambda_2)$. Moreover, if a faster equilibrating state happens to be initially further away from the steady state than a typical state, then the distance of the two states measured with some function M will cross in time and this is called a strong Mpemba effect. If the fast equilibrating states have small but nonvanishing overlap with the slowest-decaying mode, the speedup will not be exponential, and the crossing indicates a weaker Mpemba effect. To set the stage for the following examples, we first review athermality, the RT relevant to the thermal Mpemba effect.

A. Athermality as a resource

Athermality, as anticipated for classical system in Sec. I A, a state's deviation from thermal equilibrium $\hat{\pi}_\beta$, carries useful nonequilibrium free energy $\Delta F(\hat{\rho})=F(\hat{\rho})-F(\hat{\pi}_\beta)=\beta^{-1}S(\hat{\rho}\|\hat{\pi}_\beta)$, where $F(\hat{\rho})=\mathrm{Tr}(\hat{H}_s\hat{\rho})-\beta^{-1}S(\hat{\rho})$ [44]. In the resource theory of athermality, it quantifies the resource that can be converted into work using thermal operations [45,46] (defined more precisely below). These consist of operations that can be realized by coupling the system to an ancilla prepared in the Gibbs state at inverse temperature β, applying an energy-preserving unitary and tracing out the ancilla afterward, allowing heat exchange while preserving overall energy conservation. Framing the thermal Mpemba effect in this RT underscores what drives the equilibration process for the thermal Mpemba effect, even though, as with any nonequilibrium process, this free energy ultimately dissipates irreversibly into the bath rather than being fully harvested as work [47,48].

In this framework, the only free state is the thermal state at the inverse temperature β set by the environment (throughout this article, we consider $k_B=\hbar=1$); any other state is considered resourceful. A quantum channel $\mathcal{E}:\mathscr{B}(\mathscr{H}_s)\to\mathscr{B}(\mathscr{H}_s)$ [where $\mathscr{B}(\mathscr{H}_s)$ denotes the set of bounded operators on $\mathscr{H}_s$] is a free operation, denoted TO, if there exists [49]

(i) A thermal bath in a Gibbs state $\hat{\pi}_\beta=e^{-\beta\hat{H}_e}/Z_e$ with arbitrary Hamiltonian $\hat{H}_e$ and fixed inverse temperature β and
(ii) A global energy-conserving unitary $\hat{U}\in\mathscr{B}(\mathscr{H}_s\otimes\mathscr{H}_e)$ such that $[\hat{U},\hat{H}_s\otimes\hat{H}_e]=0$,

where the action of $\mathcal{E}$ on a system state $\hat{\rho}$ is given by

$$\mathcal{E}[\hat{\rho}] = \mathrm{Tr}_e[\hat{U}(\hat{\rho} \otimes \hat{\pi}_\beta)\hat{U}^\dagger]. \tag{6}$$

Trivially, Eq. (3) becomes

$$M_\alpha[\hat{\rho}(t)] = S_\alpha[\hat{\rho}_s(t)\|\hat{\pi}_\beta], \tag{7}$$

which for $\alpha \to 1$ recovers the *relative entropy of athermality*

$$M[\hat{\rho}(t)] = S[\hat{\rho}_s(t)\|\hat{\pi}_\beta]. \tag{8}$$

For states that are diagonal in the energy eigenbasis (i.e., classical states), this reduces to the KL divergence [50]. An important property is that a state $\hat{\rho}$ can be transformed into another state $\hat{\sigma}$ via TOs only if $\hat{\rho}$ thermomajorizes $\hat{\sigma}$ [51]. Notably, it was shown that, for classical Markovian thermal operations, thermomajorization can be used to determine whether the Mpemba effect occurs for *all* monotone functions [52]. In the next section, we explore examples of classical and quantum thermal Mpemba effects from the perspective of the resource theory of athermality. More generally, one can consider open system dynamics generated by a Lindbladian $\mathcal{L}$ whose unique steady state $\hat{\pi}$ need not be Gibbsian, as often studied in the context of the Mpemba effect [20,22,24,53]. In that setting, the relevant resource theory is nonstationarity, in which a state's divergence with respect to $\hat{\pi}$, i.e., $S[\hat{\rho}(t)\|\hat{\pi}]$, quantifies its resourcefulness. We discuss the framework of nonstationarity, which is directly applicable to a class of Mpemba effects in driven granular gases [9,13,14], in Appendix A. To illustrate the role of athermality in the thermal Mpemba effect, we now turn to two paradigmatic examples: a classical system akin to that in Ref. [5] and a quantum counterpart inspired by Ref. [26]. In Appendix B, we instead demonstrate how this phenomenon can arise in isolated settings. In Ref. [54], an alternative resource-theoretic interpretation of the thermal Mpemba effect is developed, using thermomajorization to analyze the roles of correlations, coherence, non-Markovianity, and dimensionality in both classical and quantum relaxation dynamics, with water serving as a central example.

B. Example 1: Thermalization of a spin chain

The quantum resource-theoretic framework for athermality introduced above can also be applied to classical dynamics, such as, for instance, discrete-state, continuous-time Markov processes [5,9,55]. In this context, the monotone for athermality Eq. (7), i.e., the KL divergence, has already been studied. The KL divergence serves as a generalized free energy: It is nonincreasing under any stochastic map preserving the steady state $\boldsymbol{\pi}_\beta$, and its decay is due to the depletion of classical athermality.

Consider a classical system whose state is specified by a probability distribution

$$\mathbf{p}(t) = \begin{pmatrix} p_1(t) \\ p_2(t) \\ \vdots \\ p_L(t) \end{pmatrix}, \tag{9}$$

where the subscript $i = 1, 2, \ldots, L$ labels discrete microstates. For the classical Markovian Liouvillian dynamics

$$\frac{\mathrm{d}\mathbf{p}(t)}{\mathrm{d}t} = \hat{\mathcal{L}}^{\mathrm{cl}}\mathbf{p}(t), \tag{10}$$

the fixed point is the thermal distribution $\mathbf{p}(t \to \infty) = \boldsymbol{\pi}_\beta$ at the inverse temperature β if the classical Liouvillian matrix $\hat{\mathcal{L}}^{\mathrm{cl}}$ is

$$\hat{\mathcal{L}}^{\mathrm{cl}}_{ii'} = \begin{cases} W_{ii'}, & i \neq i', \\ -\sum_{i \neq i'} W_{ii'}, & i = i'. \end{cases} \tag{11}$$

Here, $W_{ii'}$ satisfies the classical detailed balance condition $W_{ii'}/W_{i'i} = e^{-\beta(E_i - E_{i'})}$, where E_i denotes the energy of the ith microstate. Note that the diagonal terms ensure probability conservation in the system. It can be shown that $\hat{\mathcal{L}}^{\mathrm{cl}}$ is Hermitian with respect to the $\boldsymbol{\pi}_\beta$-weighted inner product, and it is useful to sort its eigenvalues λ_k and its corresponding eigenmodes $\mathbf{r}_k$ as $0 = \lambda_1 > \lambda_2 > \cdots$. Following Ref. [5], we study a classical spin-1/2 chain, where an upward- and a downward-pointing spin on site n is described by $s_n = +1$ and $s_n = -1$, respectively. We study N_s spins interacting locally with their nearest neighbors with coupling J and with a homogeneous external magnetic field with interaction strength h, for which the energy of a microstate reads

$$E_i = -J\sum_{n=1}^{N_s} s_n s_{n+1} - h\sum_{n=1}^{N_s} s_n, \tag{12}$$

where the microstate index $i \in \{0, 1, \ldots, 2^{N_s} - 1\}$ uniquely labels the configuration $(s_1, s_2, \ldots, s_{N_s})$ via binary encoding. We consider fixed boundary conditions $s_{N_s+1} = s_1 = +1$ and study the Liouvillian dynamics in Eq. (10) by plugging Eq. (12) into Eq. (11) under the constraint of allowing only transitions between microstates i and i' that differ by a single spin flip. Different from Ref. [5], for a given initial probability distribution $\mathbf{p}(t_0)$, we construct the fastest-thermalizing, unitarily connected state. This is the permutation of the initial $\mathbf{p}$ that minimizes the overlap with the slowest-decaying modes of $\hat{\mathcal{L}}^{\mathrm{cl}}$. Since the number of permutations grows factorially with the number of

microstates, we resort to a Metropolis algorithm outlined in Ref. [26] to minimize the cost function

$$C = \sum_{k=2}^{K+1} |\langle \mathbf{p}, \mathbf{r}_k \rangle_{\boldsymbol{\pi}_\beta}|, \tag{13}$$

describing the overlap of the initial state with $K < L-1$ slowest-decaying modes, with

$$\langle \mathbf{p}, \mathbf{r}_k \rangle_{\boldsymbol{\pi}_\beta} = \sum_i \frac{p_i (\mathbf{r}_k)_i}{(\boldsymbol{\pi}_\beta)_i} \tag{14}$$

being the so-called Markovian inner product [56].

In short, at every iteration, we perform stochastic permutations of four randomly selected spins and always accept the new configuration if the cost function C' is decreased. To avoid local minima, if $C' > C$, we still accept the new configuration with a probability $p_{\text{acc}} = \exp[-T_{\text{eff}}(C'-C)]$, where the effective inverse temperature T_{eff} is decreased linearly with the number of successful iterations. Note that such optimized (nonequilibrium) initializations are significantly more challenging to prepare experimentally, since, unlike thermal states, they require control over individual spins [57].

For the thermal operation generated by $\hat{\mathcal{L}}^{\text{cl}}$, the monotone defined in Eq. (8) simplifies to the KL divergence

$$M[\mathbf{p}(t)] = D[\mathbf{p}(t)\|\boldsymbol{\pi}_\beta] = \sum_i p_i(t) \ln\left(\frac{p_i(t)}{(\boldsymbol{\pi}_\beta)_i}\right), \tag{15}$$

which measures the divergence of $\mathbf{p}(t)$ with respect to the thermal state. The state can be decomposed as

$$\mathbf{p}(t) = \sum_{k\geq 1} a_k \mathbf{r}_k e^{\lambda_k t}, \qquad a_k = \langle \mathbf{p}, \mathbf{r}_k \rangle_{\boldsymbol{\pi}_\beta}, \tag{16}$$

and, asymptotically, the behavior of the KL divergence will be

$$D[\mathbf{p}(t)\|\boldsymbol{\pi}_\beta] \sim \frac{1}{2}|a_2|^2 e^{2\text{Re}(\lambda_2)t}, \tag{17}$$

as shown in Appendix C. In other words, the KL divergence decays exponentially with a rate being twice the spectral gap $-\text{Re}(\lambda_2)$. When the initially more resourceful state has zero overlap with the slowest-decaying mode, we are guaranteed to find a Mpemba crossing. Instead, Eq. (17) allows us to assess whether a crossing will happen also in the context of a weak Mpemba effect (i.e., diminished but not vanishing overlap with the slowest-decaying mode for the initially more resourceful state).

In Fig. 2, we show the dynamics of the KL divergence during a cooling process for a thermal state at inverse temperature β' (full line) and an optimized state (dashed line) whose overlap with the two slowest-decaying modes of the Liouvillian was minimized. The optimized state is initially further away from the equilibrium state but thermalizes exponentially faster, displaying an Mpemba crossing .

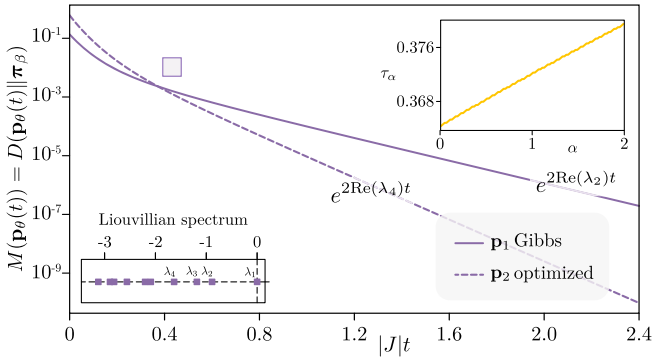

FIG. 2. The thermal Mpemba effect in an open classical system . For a classical spin chain described by Eq. (11), we study the KL divergence between the nonequilibrium distribution and the thermal state at β' during the thermalization dynamics. Upper-right inset: the crossing times between a thermal and an optimized state for the α divergence Eq. (18) as a function of α. Lower-left inset: the ten eigenvalues of the classical Liouvillian $\hat{\mathcal{L}}^{\text{cl}}$ closest to zero. The second and the fourth eigenvalue determine the asymptotic decay rate of the KL divergence for the thermal and the optimized state, respectively. We chose the parameters $J = -0.4$, $h = 0.2$, $N_s = 7$, the initial inverse temperature $\beta' = 0.5$, and the bath inverse temperature $\beta = 1$ and reduce the cost function Eq. (13) to $C \approx 2 \times 10^{-5}$ for the optimized state.

Similarly to Eq. (7), the KL divergence can be generalized to a one-parameter family of functions that are also nonincreasing under Markovian dynamics, known as the Rényi relative entropies [58]:

$$\begin{aligned} M_\alpha[\mathbf{p}(t)] &= D_\alpha[\mathbf{p}(t)\|\boldsymbol{\pi}_\beta] \\ &= \frac{1}{\alpha-1}\ln\left(\sum_i p_i^\alpha (\boldsymbol{\pi}_\beta)_i^{1-\alpha}\right), \end{aligned} \tag{18}$$

which correspond to the classical version of Eq. (7). The upper-right inset in Fig. 2 shows that the Mpemba crossing time τ_α between the thermal and optimized states increases monotonically with α. This illustrates that τ_α lacks intrinsic physical significance, as it depends on the choice of divergence measure. In particular, the variation of τ_α with α implies that different α divergences can yield qualitatively different conclusions: For certain values of α, no crossing may be detected, as we demonstrate in Appendix D. We stress that this argument relies on allowing for general nonequilibrium initial states.

C. Example 2: The Davies map

The generalization of Eq. (10) to quantum systems is given by the Lindblad equation

$$\frac{\mathrm{d}\hat{\rho}_s(t)}{\mathrm{d}t} = \mathcal{L}[\hat{\rho}_s(t)]. \tag{19}$$

Here, the superoperator $\mathcal{L} = \mathscr{H}_s + \mathcal{D}$ evolving the state $\hat{\rho}_s$ consists of a unitary part $\mathscr{H}_s[\hat{\rho}_s(t)] = -i[\hat{H}_s, \hat{\rho}_s(t)]$, where $\hat{H}_s$ denotes the system Hamiltonian, and a dissipative part

$$\mathcal{D}[\hat{\rho}_s(t)] = \sum_l \hat{L}_l \hat{\rho}_s(t) \hat{L}_l^\dagger - \frac{1}{2}\left\{\hat{L}_l^\dagger \hat{L}_l, \hat{\rho}_s(t)\right\}, \quad (20)$$

with the jump operators $\hat{L}_l$ describing the effect of an environment on the system. Here, we focus on a Lindbladian describing the weak interaction of a system with a Markovian heat bath, known as the Davies map [59], which is an important example of an elementary Markovian quantum thermal operation [60]. The Davies generator is characterized by two mathematical properties: It satisfies the quantum detailed balance condition [61], and the superoperators corresponding to the unitary and the dissipative parts of its generator commute. These properties imply that the thermal (Gibbs) state $\hat{\pi}_\beta = e^{-\beta \hat{H}_s}/\mathrm{Tr}[e^{-\beta \hat{H}_s}]$ is a fixed point of the corresponding Davies map; moreover, under standard irreducibility/ergodicity assumptions (i.e., when the semigroup is primitive), this fixed point is unique (see [62]). Moreover, in the energy eigenbasis, the Davies generator can be written in a block-diagonal form, where one block describes the thermalization of the populations and the other the thermalization of the coherences, which evolve independently from one another (as we analyze thoroughly in Sec. III C). In Ref. [26], the block structure of the Davies map was exploited to investigate the thermal Mpemba effect. In particular, it was shown that, for any initial state with nonvanishing coherences in the energy eigenbasis, one can always construct an exact unitary transformation $\hat{R}_{\mathrm{coh}}$ that leads to exponentially faster thermalization, provided that the Liouvillian gap is defined by an eigenvalue with a nonvanishing imaginary part, i.e., $\mathrm{Im}(\lambda_2) \neq 0$. At the same time, a population inversion of the rotated state, implemented by another unitary transformation $\hat{R}_{\mathrm{inv}}$, always increases the state's nonequilibrium free energy

$$F(\hat{\rho}) = \mathrm{Tr}[\hat{\rho}\,\hat{H}] - \beta^{-1} S(\hat{\rho}). \quad (21)$$

A key aspect of this fundamental thermodynamic quantity is that its (positive) deviation from the equilibrium free energy is proportional to the relative entropy of athermality [44]:

$$\begin{aligned}\Delta F(t) &= \beta^{-1} M[\hat{\rho}_s(t)] \\ &= \beta^{-1}\{F[\hat{\rho}_s(t)] - F(\hat{\pi}_\beta)\} = \beta^{-1} S[\hat{\rho}_s(t)\|\hat{\pi}_\beta], \end{aligned} \quad (22)$$

where the M is the monotone defined in Eq. (8). Crucially, Eq. (22) decreases monotonically during the Davies dynamics (see Appendix E for details on the Davies map).

By decomposing the state in the eigenmodes of $\mathcal{L}$ similarly to Eq. (16), one finds

$$\hat{\rho}(t) = \sum_{k\geq 1} a_k \hat{r}_k e^{\lambda_k t}, \qquad a_k = \mathrm{Tr}\left[\hat{\ell}_k^\dagger \hat{\rho}\right], \quad (23)$$

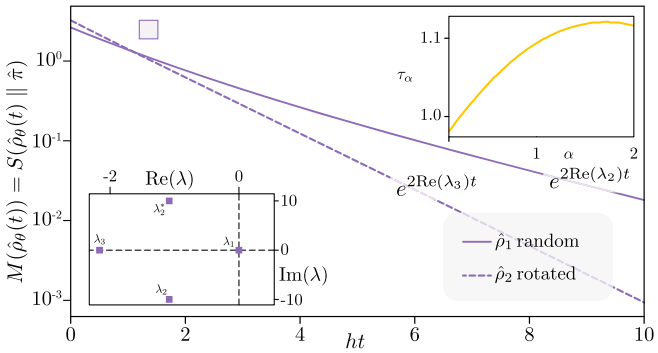

FIG. 3. The thermal Mpemba effect in an open quantum system. We consider the thermalization of a single qubit described by the Davies map [59]. For the state rotated with the unitary transformation outlined in Ref. [26] (dashed line), $M[\hat{\rho}_\theta(t)]$ [see Eq. (22)] decreases exponentially faster than for a random initial state (full line), displaying an Mpemba crossing. Upper-right inset: for the same two states, the Mpemba crossing time τ_α of the Rényi relative entropy $M_\alpha[\hat{\rho}_\theta(t)]$ [Eq. (3)] varies with α. Lower-left inset: different from the classical Liouvillian considered in Fig. 2, the spectrum of the Davies generator also features complex eigenvalues. We considered the qubit frequency $h = 10$, the bath temperature $\beta = 0.1$, a random initial state defined by the Bloch vector $\mathbf{r} = (0.221, 0.867, 0.206)$, and an optimized state with Bloch vector $\mathbf{r}' = (0, 0, 0.919)$.

which for long times (as we derive in Appendix C) implies

$$S[\hat{\rho}(t)\|\hat{\pi}_\beta] \sim \frac{1}{2}|a_j|^2 e^{2\mathrm{Re}(\lambda_j)t} \mathrm{Tr}\left[\hat{r}_j^\dagger \hat{\pi}_\beta^{-1} \hat{r}_j\right], \quad (24)$$

where $j = \arg\max_{j:a_j\neq 0} \mathrm{Re}(\lambda_j)$ labels the slowest-decaying mode of $\mathcal{L}$ with nonzero overlap with the initial state. Following Ref. [26], as an example, we consider the Davies map for a single qubit with $\hat{H}_s = h/2\hat{\sigma}^z$. In Fig. 3, we study $\Delta F(t)$ for a random initial state (full line) and its corresponding unitarily optimized state (dashed line), which shows the occurrence of a thermal Mpemba effect. We also consider the monotones defined in Eq. (7) in the upper-right inset in Fig. 3 displaying the Mpemba crossing times as a function of α. As in the classical case discussed in Sec. II B, the variation in crossing times τ_α illustrates that the presence or absence of the Mpemba effect depends on the choice of monotone [52,63], which we also elaborate on in Appendix D. Furthermore, the dependence of the Mpemba effect on the monotone function is highlighted in Appendix F, where we study the Mpemba effect using different quantum Fisher information (QFI) variants [64–67]. Note that, in Appendix B, we demonstrate that a quantum thermal Mpemba effect can also arise in a subsystem of an initially pure state evolving under an ergodic Hamiltonian, consistent with the expectations of eigenstate thermalization hypothesis (ETH).

III. THE SYMMETRY MPEMBA EFFECT

Besides the thermal Mpemba effect, a related phenomenon has recently drawn attention: the anomalous dynamical restoration of symmetries, first investigated by Ares, Murciano, and Calabrese [33]. They considered unitary dynamics generated by a Hamiltonian with a continuous symmetry, where the system is initialized in a state that breaks it. For a subsystem, the symmetry is (partially) restored during the dynamics, with the remainder of the system acting as a non-Markovian environment. In this context, the Mpemba effect ◯ is said to occur when stronger initial symmetry breaking leads to faster symmetry restoration and the degree of asymmetry is captured by the entanglement asymmetry [33]. Instances of this effect have been observed in both integrable [68–71] and nonintegrable [72–74] systems and have been confirmed experimentally [75]. In integrable systems, a compelling physical mechanism underlying the emergence of the Mpemba effect has been identified in Ref. [68]. The key idea is that symmetry restoration is mediated by the spreading of quasiparticles that propagate with different velocities. Consequently, if the dynamics of the initially more asymmetric state involves smaller contributions from the slowest-propagating quasiparticles than those of the initially less asymmetric state, their asymmetry monotones will cross in time. This type of analysis have been applied to the Mpemba effects for the non-Markovian evolution, with a finite-size environment. We, therefore, believe this applies seamlessly to our non-Markovian circuits in Secs. III G 1 and III G 2.

To explain the occurrence of the Mpemba effect in this setting, we first review symmetries in (open) quantum systems in Sec. III A. We then discuss the resource of asymmetry in Sec. III B and introduce modes of asymmetry, a useful tool for decomposing the dynamics, in Sec. III C. We show the appearance of the effect first using a classical Markov chain in Sec. III D and its quantum version in Sec. III E, then a Davies map in Sec. III F, and then in scenarios more closely aligned with existing literature: quantum circuits, both interacting with Markovian and with non-Markovian environments with U(1) symmetry, as well as systems with non-Abelian [SU(2)] symmetries in Sec. III G.

A. Symmetries in quantum systems

In closed systems, Noether's theorem [76] states that each symmetry implies the conservation of a corresponding physical charge [77,78]. When considering isolated quantum systems [79], the dynamics are governed by a unitary evolution operator $\hat{T} \in \mathscr{B}(\mathscr{H}_s)$. Let G be a group with unitary representation $\{\hat{U}_g\}_{g\in \mathrm{G}} \subset \mathscr{B}(\mathscr{H}_s)$. An operator $\hat{T}$ is called G-invariant if

$$[\hat{T}, \hat{U}_g] = 0 \quad \forall \ g \in \mathrm{G}, \tag{25}$$

or, equivalently, $\hat{T} = \hat{U}_g^\dagger \hat{T} \hat{U}_g \ \forall\, g \in \mathrm{G}$. In many cases of interest in physics, the group G is a continuous one-parameter family represented by unitaries of the form

$$\hat{U}_g = e^{i s_g \hat{Q}}, \qquad s_g \in \mathbb{R}, \tag{26}$$

where the s_g provides a group coordinate, while $\hat{Q}$ is a Hermitian operator, which will be conserved by all G-invariant unitary transformations, i.e., $\hat{T}\hat{Q}\hat{T}^\dagger = \hat{Q}$ for all G-invariant $\hat{T}$. This is an example of a connected Lie group. More generally, connected Lie groups of higher dimension, such as SU(d), have unitary representations given by

$$\hat{U}_g = e^{i \sum_{\lambda=1}^{\Lambda} s_g^\lambda \hat{Q}_\lambda}, \qquad \mathbf{s}_g^\lambda \in \mathbb{R}, \tag{27}$$

where $\{\hat{Q}_\lambda\}$, $\lambda = 1, \ldots \Lambda$, form a Lie algebra and are, in particular, closed under commutation:

$$[\hat{Q}_a, \hat{Q}_b] = i \sum_{\lambda=1}^{\Lambda} \varepsilon_{ab}^\lambda \hat{Q}_\lambda, \tag{28}$$

for real ε_{ab}^λ. In spin systems, four paradigmatic continuous symmetries are commonly encountered.

(i) Magnetization conservation [phase symmetry, group U(1)]:

$$\hat{U}_g = e^{i\gamma_g \hat{S}_z}, \qquad \gamma_g \in [0, 4\pi), \tag{29}$$

with $\hat{S}_z = \sum_n \hat{s}_n^z$ the total spin-$\frac{1}{2}$ magnetization about the z axis. In spin-$\frac{1}{2}$ chains, this U(1) symmetry is formally identical to particle-number conservation in fermionic or hard-core bosonic models.

(ii) Total angular momentum conservation, associated with the rotation group SO(3) or its double cover, the group SU(2), is

$$\hat{U}_g = e^{i\theta_g \hat{\mathbf{n}}_g \cdot \hat{\mathbf{S}}}, \qquad \theta_g \in [0, 4\pi), \qquad \hat{\mathbf{n}}_g \in \mathbb{R}^3, \tag{30}$$

where $\hat{\mathbf{n}}_g \cdot \hat{\mathbf{n}}_g = 1$ with $\hat{\mathbf{S}} = (\hat{S}_x, \hat{S}_y, \hat{S}_z)$, $\hat{S}_\alpha = \sum_n \hat{s}_n^\alpha$, $\alpha = x, y, z$.

(iii) Energy conservation (time-translation symmetry):

$$\hat{U}_g = e^{i t_g \hat{H}_s}, \qquad t_g \in \mathbb{R}. \tag{31}$$

Here, $\hat{H}_s$ is the system Hamiltonian, and t represents time, linking this unitary operator to time-translation symmetry. In the special case where the ratios of energy levels are all rational numbers, that is, when the system's time evolution is periodic, this group of unitaries is isomorphic to U(1). Otherwise, for a nonperiodic system, it is isomorphic to $\mathbb{R}$ [80].

(iv) Another important continuous symmetry, which we do not explore further, is that associated with momentum conservation (space-translation symmetry, group $\mathbb{R}^3$):

$$\hat{U}_g = e^{i\mathbf{v}_g\cdot\hat{\mathbf{P}}}, \qquad \mathbf{v}_g \in \mathbb{R}^3, \tag{32}$$

where $\hat{\mathbf{P}} = (\hat{P}_x, \hat{P}_y, \hat{P}_z)$ is the momentum operator in the three-dimensional space and $\hat{P}_\alpha = -i\partial_\alpha$, $\alpha = x, y, z$, in position space. Instead, we consider its discrete version. Consider a 1D equispaced lattice with periodic boundary condition on N sites, the symmetry group is $\mathbb{Z}_N$, realized by the translation operator

$$\hat{U}_g = e^{ik_g\hat{P}}, \qquad k_g \in \{0, 1, \ldots, N-1\}, \tag{33}$$

where $e^{i\hat{P}}$ is effectively the space-translation operator with unit lattice constant. Recently, the Mpemba effect has been found in this setting for qudits [81]. We note that for parity symmetry, associated with the group $\mathbb{Z}_2$, despite a thorough investigation [73,82], the Mpemba effect has not been unambiguously observed.

A symmetry group G acts on density matrices $\hat{\rho}$ via the unitary representation

$$\mathcal{U}_g[\hat{\rho}] = \hat{U}_g\hat{\rho}\hat{U}_g^\dagger, \qquad g \in \mathrm{G}. \tag{34}$$

States invariant under every $\mathcal{U}_g$ are called G-invariant. Given any state $\hat{\rho}$, its G-invariant component is extracted by the twirling map

$$\mathcal{G}[\hat{\rho}] = \int_G \mathrm{d}g\mathcal{U}_g[\hat{\rho}] = \int_G \mathrm{d}g\hat{U}_g\hat{\rho}\hat{U}_g^\dagger, \tag{35}$$

where $\mathrm{d}g$ denotes the normalized Haar measure on G and we have assumed the group G is compact. This CPTP map projects any input state onto its symmetric component by averaging over all group actions. For finite groups, this becomes

$$\mathcal{G}[\hat{\rho}] = \frac{1}{|G|}\sum_{g\in\mathrm{G}}\mathcal{U}_g[\hat{\rho}]. \tag{36}$$

As previously mentioned, the Mpemba effect occurs when the system interacts with an environment. If we, therefore, consider the G-invariant operator $\hat{T}$ of Eq. (25) as the evolution operator on $\mathscr{H}_s \otimes \mathscr{H}_e$, its local action on $\mathscr{H}_s$ will preserve only a weaker form of symmetry, as follows. In fact, let $\mathcal{E}$ be a map defined as

$$\mathcal{E}[\cdot] = \mathrm{Tr}_e\{\hat{T}([\cdot]\otimes\hat{\pi}_e)\hat{T}^\dagger\}, \tag{37}$$

with $\hat{\pi}_e$ a G-invariant state on $\mathscr{H}_e$. Then, it can be easily shown (see Appendix G) that, because the initial state of $\mathscr{H}_e$ and the global unitary time evolution $\hat{T}$ respect the symmetry, the time evolution of the reduced system also respects the symmetry; that is, it satisfies the G-covariance condition, also known as weak symmetry [79,83], namely,

$$\mathcal{E}\circ\mathcal{U}_g[\hat{\rho}] = \mathcal{U}_g\circ\mathcal{E}[\hat{\rho}] \quad \forall\, g\in\mathrm{G}, \quad \forall\,\hat{\rho}. \tag{38}$$

Conversely, it has been shown that any CPTP map that respects this covariance condition can be realized via Eq. (37), using a G-invariant unitary $\hat{T}$, and a G-invariant state $\hat{\pi}_e$ [84–86]. Therefore, while the global evolution is a G-invariant unitary transformation, the dynamics of the reduced state of the system is governed by a G-covariant CPTP map. As a result, the asymmetry (i.e., symmetry breaking) with respect to the group G can decrease. This can be quantified by means of the asymmetry monotones M, i.e., functions satisfying

$$M(\mathcal{E}[\hat{\rho}]) \le M(\hat{\rho}) \quad \forall\,\hat{\rho}\in\mathscr{S}(\mathscr{H}_s) \tag{39}$$

for any G-covariant $\mathcal{E}$ map. Hence, while for open systems the presence of symmetry does not imply conservation laws, that is, Noether's theorem is not applicable, asymmetry monotones still capture nontrivial implications of symmetries [67]. In generic open system dynamics that respect the symmetry, the asymmetry (symmetry breaking) in the initial state decreases, although the complete restoration of the symmetry is not *a priori* guaranteed [87]. In the special case of closed system dynamics, the presence of symmetry implies the conservation of all asymmetry monotones. That is, for any G-invariant unitary $\hat{T}$, $M(\hat{T}\hat{\rho}\hat{T}^\dagger) = M(\hat{\rho})$: In this regime, no asymmetry can be created or destroyed. To observe Mpemba effects, thus, one clearly needs to consider G-covariant maps, i.e., systems interacting with environments.

When G is the one-parameter group of time translations generated by the system Hamiltonian $\hat{H}_s$, the covariant operations are precisely the time-translation-invariant (also called phase-covariant) maps. An example of such maps is the TO, defined in Sec. II A. The notion of energetic coherence in quantum thermodynamics, that is, superpositions of states with different energies, can be understood as asymmetry with respect to time translations [37,46,90]. Note that, although asymmetry under time translations is globally conserved under general energy-conserving unitaries, the reduced map can still dephase in the energy basis, effectively restoring the symmetry by erasing coherence (see Sec. III F for further discussion). In the open systems literature, the covariance condition is often referred to as weak symmetry, to distinguish it from a stronger notion, known as strong symmetry [79,83], in which all the Kraus operators of the channel are G-invariant (i.e., commute with the group action) [91]. Weak symmetry

[G covariance, Eq. (38)] admits nonincreasing asymmetry monotones, whereas strong symmetry [G invariance, Eq. (25)] guarantees conserved charges in the dynamics.

Under the restriction to G-covariant operations, any state exhibiting asymmetry cannot be generated for free and must instead be supplied externally as a resource. The greater the asymmetry of this resource state, the more power it confers for tasks that require breaking the symmetry. For instance, in the case of U(1) symmetry, the precision in probing the phase of a U(1) rotation increases as the state becomes more tilted with respect to the z direction, as quantified by Eq. (5) or, for example, by the Wigner-Yanase skew information (see Appendix F). Similarly, tasks such as aligning reference frames or achieving quantum-enhanced measurements beyond the shot-noise limit benefit from using more asymmetric states [92,93]. In this sense, asymmetry becomes a useful resource.

B. Asymmetry as a resource

For any symmetry group G, the resource theory of asymmetry with respect to G assumes that all systems under consideration are equipped with a representation of the group. The set of free states and free operations in this resource theory are then defined as those that respect the symmetry [43,67,85,94].

In particular, for any system s with Hilbert space $\mathscr{H}_s$, the free states are the G-invariant states

$$\mathscr{F} = \{\hat{\rho} \in \mathscr{B}(\mathscr{H}_s) | \mathcal{G}[\hat{\rho}] = \hat{\rho}\}, \tag{40}$$

where G denotes the corresponding twirling map.

Free operations on system s are CPTP maps $\mathcal{E}$ satisfying the covariance condition

$$\mathcal{E} \circ \mathcal{U}_g = \mathcal{U}_g \circ \mathcal{E} \quad \forall\, g \in \mathrm{G}.$$

Note that, as required in all resource theories, free operations (i.e., G-covariant maps) map free states (i.e., G-invariant states) to free states.

A useful monotone in this resource theory is the *relative entropy of asymmetry* [95,96]:

$$\begin{aligned} M(\hat{\rho}) &= \min_{\hat{\pi} \in \mathscr{F}} S(\hat{\rho} \| \hat{\pi}) \\ &= S(\hat{\rho} \| \mathcal{G}[\hat{\rho}]) \\ &= S(\mathcal{G}[\hat{\rho}]) - S(\hat{\rho}), \end{aligned} \tag{41}$$

which corresponds to Eq. (5). (The quantity $S(\mathcal{G}[\hat{\rho}]) - S(\hat{\rho})$ was first introduced in Ref. [96], under the name "asymmetry.") This quantifies the minimal divergence of $\hat{\rho}$ with respect to the manifold of symmetric states. Intuitively, if $\hat{\rho}$ is nearly invariant, twirling induces little entropy change; if $\hat{\rho}$ breaks the symmetry strongly, mixing over G spreads its support and increases entropy substantially [67]. The relative entropy of asymmetry can be extended to the α divergences of Eq. (3) as the α divergences of asymmetry for $\alpha \in (0,1) \cup (1,2]$. All these maps are guaranteed to be monotonic for G-covariant maps [67]. An alternative family of monotones is the QFI, which we discuss in Appendix F.

C. Modes of asymmetry

Within the resource theory of asymmetry, an important tool to characterize the symmetry breaking was introduced in Ref. [37]: the modes of asymmetry. In this section, we outline the main ingredients to this concept, a simple example, and how this idea can be used to fully understand the symmetry Mpemba effect.

Consider a finite or compact Lie group G acting unitarily on $\mathscr{H}_s$ via $\hat{U}\colon G \to \mathscr{B}(\mathscr{H}_s)$. The full operator algebra $\mathscr{B}(\mathscr{H}_s)$ then carries an induced adjoint action of G and the irreducible representation of G labeled by μ, which appears with multiplicity m_μ in $\mathscr{B}(\mathscr{H}_s)$. One can use the irreducible tensor operator basis $\{\hat{T}_\alpha^{(\mu,q)}\}$ of $\mathscr{B}(\mathscr{H}_s)$, $q = 1, \ldots, d_\mu$ (d_μ dimension of the irrep, namely, an irreducible representation) and $\alpha = 1, \ldots, m_\mu$ satisfying $\mathrm{Tr}[\hat{T}_\alpha^{(\mu,q)\dagger} \hat{T}_\beta^{(\nu,\ell)}] = \delta_{\mu\nu}\delta_{q\ell}\delta_{\alpha\beta}$, to decompose any operator $\hat{X} \in \mathscr{B}(\mathscr{H}_s)$ as

$$\hat{X} = \sum_{\mu,q} \hat{X}^{(\mu,q)}. \tag{42}$$

Here, $\hat{X}^{(\mu,q)}$ is the (μ, q) mode of $\hat{X}$, defined as

$$\hat{X}^{(\mu,q)} = \sum_\alpha \mathrm{Tr}[\hat{T}_\alpha^{(\mu,q)\dagger} \hat{X}] \hat{T}_\alpha^{(\mu,q)}. \tag{43}$$

A basis-independent way to define these modes is by the group's action

$$\hat{X}^{(\mu,q)} = d_\mu \int_G \mathrm{d}g D_{qq}^{(\mu)*}(g) \mathcal{U}_g[\hat{X}], \tag{44}$$

where $D_{\ell q}^{(\mu)}(g) = \langle \mu, \ell | \hat{U}_g | \mu, q \rangle$. We write $\mathscr{H}^{(\mu,q)}$ for the subspace where the (μ, q) mode lives. Assuming $\mu = 0$ corresponds to the trivial irrep, with $d_\mu = 1$, one has $D_{00}^{(0)}(g) = 1$, from which it becomes evident how the mode associated with the trivial irrep corresponds to the twirled part of the operator, as in Eq. (35). By orthonormality of the $\{\hat{T}_\alpha^{(\mu,q)}\}$ basis, it also follows that all the other modes will characterize a symmetry breaking. For discrete groups, Eq. (44) becomes

$$\hat{X}^{(\mu,q)} = \frac{d_\mu}{|G|} \sum_{g \in \mathrm{G}} D_{qq}^{(\mu)*}(g) \mathcal{U}_g[\hat{X}]. \tag{45}$$

This formalism becomes particularly useful when the system evolves by the free operations of the resource

theory of asymmetry. Specifically, following Ref. [37], a map $\mathcal{E}$ is G-covariant iff it acts within each μ sector as

$$\mathcal{E}[\hat{X}^{(\mu,q)}] = (\mathcal{E}[\hat{X}])^{(\mu,q)}. \tag{46}$$

Namely, each mode evolves independently and so, since the asymmetry can decrease only by G-covariant maps and the trace norm respects the data processing inequality, the trace norm of each asymmetry mode is individually a monotone, that is,

$$\|\mathcal{E}[\hat{X}^{(\mu,q)}]\|_1 \leq \|\hat{X}^{(\mu,q)}\|_1. \tag{47}$$

As a concrete example, consider the symmetry group $G = \mathrm{U}(1)$, generated by the total-z magnetization operator $\hat{S}_z$ on N_s spin-half particles. Its unitary representation is as in Eq. (29) given by $\hat{U}_\gamma$ with $\gamma \in [0, 4\pi)$.

Because of the group's simple structure, its asymmetry modes are labeled by a single integer μ, which determines the U(1) irrep as $D^{(\mu)}$: $e^{i\theta} \mapsto e^{i\mu\theta}$. The operator $\hat{S}_z$ is diagonal in the computational basis $\{|0\rangle, |1\rangle\}^{\otimes N_s}$, with eigenvalues $\pm\frac{1}{2}, \ldots, \pm N_s/2$ when N_s, the number of qubits, is odd, and $0, \pm 1, \ldots, \pm N_s/2$ when N_s is even. We can equivalently label the elements of the computational basis as $\{|m, \alpha\rangle\}$, where m is the eigenvalue of $\hat{S}_z$ and α is a multiplicity index. In particular, m is simply half the difference between the number of 0's and 1's in a computational basis element.

Then, the μ component of any $\hat{\rho}$ is given by projection

$$\begin{aligned}\hat{\rho}^{(\mu)} &= \int_0^{4\pi} \frac{\mathrm{d}\gamma}{4\pi} e^{-i\gamma\mu/2}(e^{i\gamma\hat{S}_z}\hat{\rho}e^{-i\gamma\hat{S}_z}) \\ &= \sum_m \hat{\Pi}_m \hat{\rho} \hat{\Pi}_{m+\mu},\end{aligned} \tag{48}$$

where $\hat{\Pi}_m = \sum_\alpha |m, \alpha\rangle\langle m, \alpha|$ is the projection to the subspace of states with m magnetization. This can also be written as Eq. (43) in terms of the irreducible tensor basis of U(1) as

$$\hat{\rho}^{(\mu)} = \sum_\alpha \mathrm{Tr}\left[\hat{T}_\alpha^{(\mu)\dagger}\hat{\rho}\right]\hat{T}_\alpha^{(\mu)}, \tag{49}$$

where one can choose the tensor operators to be simply the outer product of two computational basis elements or, equivalently, two eigenvectors of $\hat{S}_z$:

$$\hat{T}_\alpha^{(\mu)} = |m, \alpha_1\rangle\langle m + \mu, \alpha_2|, \tag{50}$$

where $\alpha = (m, \alpha_1, \alpha_2)$. It follows that

$$e^{i\gamma\hat{S}_z}\hat{\rho}^{(\mu)}e^{-i\gamma\hat{S}_z} = e^{i\gamma\mu}\hat{\rho}^{(\mu)}, \tag{51}$$

where at $\mu = 0$ we find the symmetrized (twirled) state.

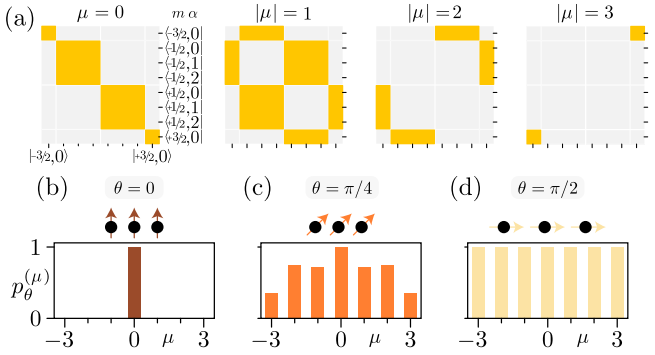

FIG. 4. U(1) symmetry sectors and mode-occupancy distributions for a three-qubit tilted states. The computational basis elements labeled as $|m, \alpha_1\rangle\langle m', \alpha_2|$ are associated to a magnetization difference $\mu = m - m'$. By reordering the eight basis operators into an 8×8 matrix by sorting rows and columns by ascendant m, we obtain the U(1) symmetry sectors shown in (a), with each block (colored in yellow) corresponding to a fixed $|\mu|$. (b)–(d) display the mode-occupancy histograms [defined in Eq. (53)] for the three tilted-ferromagnet states of Eq. (52) with $N_s = 3$: in (b) a perfectly symmetric state (only $\mu = 0$ appears), in (c) an partially asymmetric state (nonzero weight in several $\mu \neq 0$ sectors), and in (d) a maximally asymmetric state (uniform weight across all sectors).

Fixing the number of qubits to $N_s = 3$, we order the basis states by increasing m_k [see Fig. 4(a)] to find the block structure with $\mu = 0, \pm 1, \pm 2, \pm 3$. To illustrate the mode decomposition, we employ the family of tilted pure states

$$|\varphi(\theta)\rangle = \bigotimes_{n=1}^{3} e^{-i\theta\hat{s}_n^y}|0\rangle_n, \tag{52}$$

so that $\theta = 0$ gives the fully z-aligned (symmetric) state, $\theta = \pi/4$ an intermediate tilt, and $\theta = \pi/2$ the fully x-aligned (maximally asymmetric) state [Figs. 4(b)–4(d)]. Writing $\hat{\rho}_\theta = |\varphi(\theta)\rangle\langle\varphi(\theta)|$, we measure the weight of mode μ via the rescaled trace norm:

$$p_\theta^{(\mu)} = \left\|\hat{\rho}_\theta^{(\mu)}\right\|_1 \Big/ \left\|\hat{\rho}_{\pi/2}^{(\mu)}\right\|_1. \tag{53}$$

As θ increases from 0 to $\pi/2$, the weights $p_\theta^{(\mu\neq 0)}$ grow, showing that the tilted state acquires higher-μ asymmetry components.

As we discuss in the next section, this formalism helps unify the two phenomena: The thermal Mpemba effect hinges on the small overlap with the overall slowest-decaying eigenmode, whereas the symmetry Mpemba effect stems exclusively from the decay rate of the slowest eigenmode living in a ($\mu \neq 0$) sector.

D. Example 1: A classical symmetry Mpemba effect with $\mathbb{Z}_4$

To illustrate how an initially more asymmetric distribution can restore symmetry faster than a more symmetric

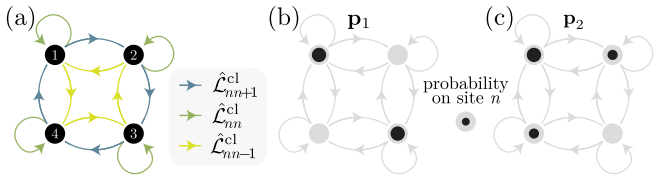

FIG. 5. (a) The generator of the classical Markov chain with the four sites arranged on a ring and three type of jumps making them interacts. (b),(c) The distributions $\mathbf{p_1}$ and $\mathbf{p_2}$, which are $(0.5, 0, 0.5, 0)^T$ and $(0.5, 0.25, 0, 0.25)^T$, respectively.

one ◯, we consider the minimal classical setup in which distinct symmetry-breaking eigenmodes (namely, eigenmodes living in $\mu \neq 0$ sectors) decay at different rates: a four-site Markov chain on a ring (represented in Fig. 5), invariant under the cyclic rotation $n \mapsto n+1 (\mathrm{mod}\ 4)$, namely, $\mathbb{Z}_4$-covariant. The irreps are $D^{(\mu)}(n) = e^{2\pi i n\mu/4} = i^{n\mu}$, where $\mu = 0, 1, 2, 3$. Jumps occur at a unit rate between each pair of neighbors, as described by the Liouvillian

$$\hat{\mathcal{L}}^{\rm cl}_{nm} = \begin{cases} 1+\varepsilon, & m = n+1 \pmod 4, \\ 1-\varepsilon, & m = n-1 \pmod 4, \\ -2, & n = m, \\ 0, & \text{otherwise}, \end{cases} \tag{54}$$

where $\varepsilon \in (-1, 1)$ is the chirality parameter. In this case, there are four modes of asymmetry, corresponding to $\mu = 0, 1, 2, 3$. Then, the analogs of tensor operators are given by

$$\mathbf{T}^{(\mu)} = \frac{1}{2}(1, i^{\mu}, i^{2\mu}, i^{3\mu})^T. \tag{55}$$

In particular, under the action of cyclic rotation $n \mapsto n+1$ (mod 4), this vector is mapped to itself, up to a phase $-i^{\mu}$. Writing the eigenmodes of $\hat{\mathcal{L}}^{\rm cl}$ in terms of the $\{\mathbf{T}^{(\mu)}\}$ basis, we get $\boldsymbol{\pi} = \mathbf{r}_1 = \mathbf{T}^{(0)}$ (eigenvalue $\lambda_1 = 0$), $\mathbf{r}_2 = \mathbf{T}^{(1)}$ ($\lambda_2 = -2 + 2i\varepsilon$), $\mathbf{r}_3 = \mathbf{T}^{(3)}$ ($\lambda_3 = -2 - 2i\varepsilon$), and $\mathbf{r}_4 = \mathbf{T}^{(2)}$ ($\lambda_4 = -4$).

Hence, for $\varepsilon \in (-1, 1)$, $\mathbf{r}_4$ is the fastest-decaying mode. (Note that the detailed balance condition is violated for $\varepsilon \neq 0$.) Each eigenmode lives in a single asymmetry sector, which guarantees the preservation of the mode structure, as in Eq. (46). Only $\boldsymbol{\pi}$ (which lives in $\mu = 0$) is fully symmetric; the three asymmetric eigenmodes, two slow ones ($\mathbf{r}_2, \mathbf{r}_3$) and one fast one ($\mathbf{r_4}$), govern how different distortions decay back to equilibrium. In this case, the relative entropy of asymmetry in Eq. (41) is equal to the KL divergence of the current distribution $\mathbf{p}(t)$ from its symmetrized version $\hat{\mathcal{G}}\mathbf{p}(t)$, adapted to this case using the discrete version of the twirling operation in Eq. (36). Since averaging over all four rotations yields the uniform state $\hat{\mathcal{G}}\mathbf{p}(t) = \boldsymbol{\pi}/2$, the relative entropy of asymmetry simplifies to

$$M[\mathbf{p}(t)] = D[\mathbf{p}(t)\|\hat{\mathcal{G}}\mathbf{p}(t)] = \sum_{k=1}^{4} p_k(t) \ln[4p_k(t)], \tag{56}$$

which vanishes precisely when $\mathbf{p}$ is uniform and decreases under the dynamics $e^{t\hat{\mathcal{L}}^{\rm cl}}$. To find a strong Mpemba effect, we compare two probability vectors chosen along orthogonal spectral directions as in Eq. (16):

$$\mathbf{p}_1 = \underbrace{\frac{1}{2}\boldsymbol{\pi}}_{\mathbf{p}_1^{(0)}} + \underbrace{\frac{1}{4}\mathbf{r}_2}_{\mathbf{p}_1^{(1)}} + \underbrace{\frac{1}{4}\mathbf{r}_3}_{\mathbf{p}_1^{(3)}}, \qquad \mathbf{p}_2 = \underbrace{\frac{1}{2}\boldsymbol{\pi}}_{\mathbf{p}_2^{(0)}} + \underbrace{\frac{1}{2}\mathbf{r}_4}_{\mathbf{p}_2^{(2)}}, \tag{57}$$

where the first lies entirely along the slow symmetry-breaking eigenmodes $\mathbf{r_2}$ and $\mathbf{r_3}$, while the second has only a component in the fast eigenmode $\mathbf{r_4}$. The underbraces highlight the mode decomposition of the states where $\mathbf{p}_{\theta}^{(\mu)} = \langle \mathbf{T}^{(\mu)}, \mathbf{p}_{\theta} \rangle_{\boldsymbol{\pi}} \mathbf{T}^{(\mu)}$ for $\theta = 1, 2$, which corresponds to the adaptation of Eq. (43) to this case. While, at $t = 0$, $0.35 \approx M(\mathbf{p}_1) < M(\mathbf{p}_2) \approx 0.69$, if we pick $\varepsilon = 1/4$, according to Eq. (17), their asymmetry behavior asymptotically decreases as

$$M[\mathbf{p}_1(t)] \sim \frac{1}{4}e^{-4t}, \qquad M[\mathbf{p}_2(t)] \sim \frac{1}{2}e^{-8t}. \tag{58}$$

By numerically propagating the two initial configurations Eq. (57) with the Liouvillian Eq. (54), we find that the two monotones M cross at time $\tau = 0.16$. In other words, the distribution $\mathbf{p}_2$ outpaces $\mathbf{p}_1$ in restoring the $\mathbb{Z}_4$ symmetry, manifesting the symmetry Mpemba effect in a classical system. In this minimal example, the eigenmodes of the Liouvillian coincide with the irreducible basis, and the uniqueness of the symmetric configuration reduces symmetry restoration to ordinary equilibration on this classical Markov chain. This simplification, however, is an artifact of our minimal model. In the next section, we turn to a richer scenario in which each eigenvalue sector μ appears with multiplicity 4. In that case, one can observe genuinely new behavior, such as nontrivial evolution within the $\mu = 0$ symmetric subspace, that cleanly separates the process of symmetry restoration from the usual equilibration dynamics.

E. Example 2: A quantum symmetry Mpemba effect with $\mathbb{Z}_4$

In the classical Markov chain of Sec. III D, the generator splits into four one-dimensional symmetry sectors under the action of $\mathbb{Z}_4$. We now construct a quantum analog: a single spinless particle hopping on a four-site ring, governed by a $\mathbb{Z}_4$-covariant Lindblad dynamics. The irreducible tensor operators are labeled by $\mu \in \{0, 1, 2, 3\}$ with multiplicity index $\alpha \in \{0, 1, 2, 3\}$:

$$\hat{T}^{(\mu)}_{\alpha} = \frac{1}{2}\sum_{n=1}^{4} e^{2\pi i n\mu/4} |n + \alpha \ (\mathrm{mod}\ 4)\rangle\langle n|. \tag{59}$$

Here, n labels the site on the ring, understood modulo 4 so that site 5 is identified with site 1 and site 0 with site 4, and the phase factor ensures each $\hat{T}_\alpha^{(\mu)}$ transforms in the μth irreducible representation of $\mathbb{Z}_4$. To define the dynamics, we embed the classical jump rates into Lindblad hopping operators and add a coherent Hamiltonian term. The master equation reads

$$\frac{d\hat{\rho}}{dt} = \mathcal{L}[\hat{\rho}] = -i[\hat{H}_s, \hat{\rho}] + \mathcal{D}_-[\hat{\rho}] + \mathcal{D}_+[\hat{\rho}], \tag{60}$$

where the coherent part of the dynamics is generated by the Hamiltonian

$$\hat{H}_s = J\sum_{n=1}^{4} |n\rangle\langle n+1 \pmod 4| + |n+1 \pmod 4\rangle\langle n|, \tag{61}$$

which describes hopping between neighboring sites on a four-site ring with amplitude J. The incoherent, biased hopping around the ring is implemented by the two dissipators [defined as Eq. (20)], respectively, for the jump operators

$$\begin{aligned} \hat{L}_{n,+} &= \sqrt{1+\varepsilon}|n+1 \pmod 4\rangle\langle n|, \\ \hat{L}_{n,-} &= \sqrt{1-\varepsilon}|n-1 \pmod 4\rangle\langle n|, \end{aligned} \tag{62}$$

where the bias parameter $\varepsilon \in [-1, 1]$, as before, tilts the rates so that $\varepsilon > 0$ enhances clockwise jumps and $\varepsilon < 0$ enhances counterclockwise jumps. This construction yields a Lindbladian $\mathcal{L}$ that is manifestly $\mathbb{Z}_4$-covariant and, thus, block-diagonal in the μ sectors.

We set $J = 1$ and $\varepsilon = 1/4$. The Lindblad superoperator $\mathcal{L}$ admits 16 eigenmodes, four for each μ sector, which can be expressed in the tensor basis $\hat{T}_\alpha^{(\mu)}$. Among these, the unique eigenmode belonging to the $\mu = 0$ sector and zero eigenvalue is the steady state $\hat{\pi}$. The remaining 15 eigenmodes $\hat{r}_k$ decay with eigenvalues λ_k, ordered by decreasing real part $\mathrm{Re}(\lambda_k)$ [97].

We prepare two initial states by mixing the steady state with selected decaying eigenmodes:

$$\begin{aligned} \hat{\rho}_1 &= \underbrace{\hat{\pi}/2 + (\hat{r}_2 - \hat{r}_3 + \hat{r}_4)/9}_{\hat{\rho}_1^{(0)}} + \underbrace{(-\hat{r}_5/5)}_{\hat{\rho}_1^{(1)}} \\ &\quad + \underbrace{(\hat{r}_{14} + \hat{r}_{15})/8}_{\hat{\rho}_1^{(2)}} + \underbrace{(-\hat{r}_{13}/5)}_{\hat{\rho}_1^{(3)}}, \\ \hat{\rho}_2 &= \underbrace{\hat{\pi}/2 + (\hat{r}_2 - 2\hat{r}_3 + \hat{r}_4)/10}_{\hat{\rho}_2^{(0)}} + \underbrace{-\hat{r}_{16}/2}_{\hat{\rho}_2^{(2)}}. \end{aligned} \tag{63}$$

These choices introduce different amounts of initial asymmetry in sectors $\mu = 1, 2, 3$. We then evolve each state under the dynamics

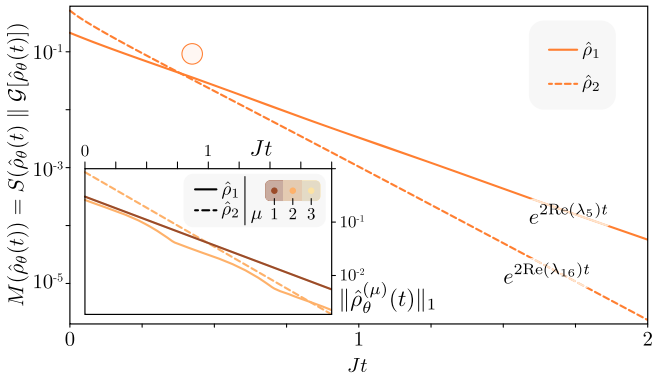

FIG. 6. Symmetry quantum Mpemba effect in a system with $\mathbb{Z}_4$ symmetry. Main panel: time evolution of the relative entropy of asymmetry $M[\hat{\rho}_1(t)]$ and $M[\hat{\rho}_2(t)]$, showing exponential decay rates given by λ_{10} and λ_{16}, respectively. Inset: trace norms $\|\hat{\rho}_1^{(\mu)}(t)\|_1$ and $\|\hat{\rho}_2^{(\mu)}(t)\|_1$ for each charge sector, illustrating that eigenmodes $\hat{r}_{10}$ and $\hat{r}_{14}$ are related by Hermitian conjugation and overlap in the $\mu = 1$ and $\mu = 3$ sectors. Each eigenmode decays exponentially in time, where the structure of $\hat{\rho}_1(t)$ causes $\|\hat{\rho}_1^{(2)}(t)\|_1$ to oscillate as it decays.

$$\hat{\rho}_\theta(t) = e^{t\mathcal{L}}[\hat{\rho}_\theta] \tag{64}$$

and quantify the restoration of $\mathbb{Z}_4$ symmetry via the relative entropy of asymmetry $M(\hat{\rho}_\theta(t))$ as defined in Eq. (41). Figure 6 shows that the state $\hat{\rho}_2$, which starts with a larger asymmetry in sector $\mu = 2$, relaxes faster than $\hat{\rho}_1$, which has its dominant asymmetry in sector $\mu = 1$ (and, equivalently, $\mu = 3$). Despite having greater initial asymmetry, $\hat{\rho}_2$ crosses below $\hat{\rho}_1$ in $M(t)$, demonstrating the symmetry Mpemba effect. The inset highlights the decay of each charge-sector norm, confirming the underlying exponential behavior of the asymmetry modes. In this example, we see a first advantage brought by the modes of asymmetry: They help identify the eigenmodes responsible for the symmetry breaking.

F. Example 3: Time-translation-symmetry Mpemba effect in Davies maps

We now turn to a continuous symmetry, namely, the time-translation symmetry. Let us consider once again a Davies map described in Sec. II C but now focusing on the symmetry Mpemba effect ◯. When the symmetry group action $e^{i\hat{H}_s t}: t \in \mathbb{R}$ is generated by the system Hamiltonian $\hat{H}_s$, the modes of asymmetry $\hat{\rho}^{(\mu)}$ of a state $\hat{\rho}$ coincide with its energy coherence blocks at Bohr frequency μ. Concretely, $\hat{\rho} = \sum_\mu \hat{\rho}^{(\mu)}$ and $\mathcal{U}_g[\hat{\rho}^{(\mu)}] = e^{i\mu t_g}\hat{\rho}^{(\mu)}$, where $\mathcal{U}_g[\cdot] = e^{i\hat{H}_s t_g}[\cdot]e^{-i\hat{H}_s t_g}$, so that $\mu = 0$ picks out all diagonal (incoherent) terms and each $\mu \neq 0$ selects the off-diagonal coherences oscillating at frequency μ under unitary time evolution. The Lindbladian eigenmodes corresponding to symmetry-preserving (symmetry-breaking)

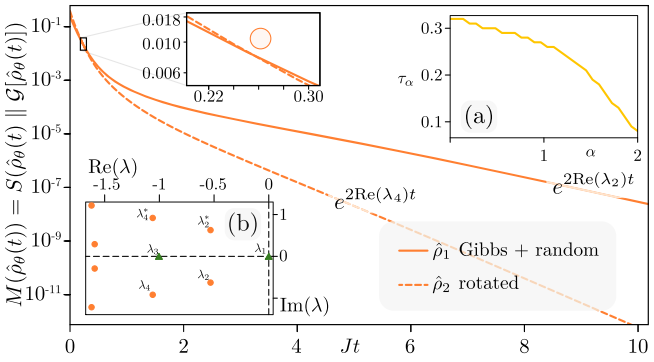

FIG. 7. Symmetry Mpemba effect in the thermalization of a spin system under the Davies map [59]. We consider a transverse field Ising model (TFIM) Eq. (65) with $J = 1$, $h = 1$, $N_s = 4$, environment temperature $\beta = 0.1$, initial thermal temperature $\beta_i = 1$, and perturbation strength $\gamma = 0.05$. Note that, differently from the previous example Eq. (62), there is no asymmetry between hopping to the left and to the right (i.e., $\varepsilon = 0$). The solid curve shows $M[\hat{\rho}_1(t)]$ for $\hat{\rho}_1 = (\hat{\rho}_{\mathrm{Gibbs}} + \gamma\hat{\rho}_{\mathrm{rand}})/N$; the dashed curve shows $M[\hat{\rho}_2(t)]$ for $\hat{\rho}_2 = \hat{R}_{\mathrm{metr}}\hat{\rho}_1\hat{R}^\dagger_{\mathrm{metr}}$, with $\hat{R}_{\mathrm{metr}}$ obtained via a Metropolis algorithm [26] to minimize overlap with the slowest-decaying eigenmode $\widehat{\ell}_2$. Inset (a): the Mpemba crossing time for the Petz-Rényi α divergences Eq. (3) for different α. Inset (b): the ten eigenvalues of the Davies generator with smallest real parts; green triangles indicate ones at $\mu = 0$ and orange circles the $\mu \neq 0$ ones.

modes are depicted in green (orange) in the lower-left inset in Fig. 7. In Davies maps, the Lindbladian $\mathcal{L}$ commutes by construction with the Hamiltonian evolution and, thus, respects the time-translation symmetry [49]. [Recall that when, up to a shift, the energy levels are all integer multiples of a fixed energy, i.e., the system dynamics is periodic, then time translation becomes isomorphic to U(1), and such maps are also referred to as phase-covariant.] As discussed in Sec. III A, this guarantees the monotonicity of the functions $M_\alpha[\hat{\rho}(t)]$. A symmetry Mpemba effect ○ occurs when the state with higher initial coherence decoheres faster than one with lower coherence, and their monotone curves cross in time.

As a concrete illustration, consider the transverse-field Ising chain

$$\hat{H}_s = -J\sum_{n=1}^{N_s-1}\hat{\sigma}^z_n\hat{\sigma}^z_{n+1} + h\sum_{n=1}^{N_s}\hat{\sigma}^x_n, \tag{65}$$

with $N_s = 4$ and open boundary conditions. We compare two unitarily connected initial states

$$\hat{\rho}_1 = (\hat{\rho}_{\mathrm{Gibbs}} + \gamma\hat{\rho}_{\mathrm{rand}})/N, \tag{66}$$

$$\hat{\rho}_2 = \hat{R}_{\mathrm{metr}}\hat{\rho}_1\hat{R}^\dagger_{\mathrm{metr}}, \tag{67}$$

where N is a normalization constant, $\hat{\rho}_{\mathrm{rand}} = \hat{X}^\dagger\hat{X}/\mathrm{Tr}(\hat{X}^\dagger\hat{X})$, with $\hat{X}$ being a random Hermitian matrix with real and imaginary components uniformly distributed in [0, 1], and $\hat{R}_{\mathrm{metr}}$ is the unitary transformation minimizing the overlap of $\hat{\rho}_1$ with $\widehat{\ell}_2$ via the Metropolis algorithm [26]. Figure 7 shows the crossing of $M[\hat{\rho}_1(t)]$ (solid line) and $M[\hat{\rho}_2(t)]$ (dashed line). Moreover, the upper-right inset indicates that, when considering the Petz-Rényi α divergences, the crossing time decreases upon increasing α. Importantly, in contrast to the thermal Mpemba effect (Sec. II C) that involves both $\mu = 0$ (populations) and $|\mu| > 0$ (coherences) blocks, here only the $|\mu| > 0$ modes contribute to the decay of $M[\hat{\rho}_1(t)]$: The slowest-decaying coherent mode corresponds to the complex eigenvalue with a real part closest to zero.

G. Example 4: Symmetry Mpemba effects in quantum circuits

Originally, the symmetry Mpemba effect was investigated in continuous-time models [33]. Here, we consider circuit models [72,73], in which time is treated as a discrete variable, and focus on two symmetries, U(1) and SU(2). We consider N qubits, with N even, where the first N_s qubits define the system and the remaining N_e the environment. The initial state spontaneously breaks the symmetry on the system qubits only, with the extent of the breaking controlled by a parameter θ. The state is then evolved by a circuit composed by gates preserving the symmetry arranged in a brickwork geometry. We consider two-qubit gates, and the Floquet unitary $\hat{U}$ is

$$\hat{U} = \prod_{n=1}^{N/2}\hat{u}_{2n-1}\prod_{n=1}^{N/2}\hat{u}_{2n}, \tag{68}$$

where $\hat{u}_n$ are gates on the n, $n+1$ qubits and $\hat{u}_N$ connects the last and the first qubits to enforce periodic boundary conditions, as represented in the two-qubit brickwork circuits in Fig. 8(b). While in the absence of symmetries any unitary can be decomposed into two local gates, when enforcing a symmetry this is not guaranteed anymore: A generic G-invariant unitary might not be composed of two-local G-invariant gates [98,99]. [For U(1) and SU(2), two-local gates suffice for semi-universality, meaning that, for states restricted to a single irrep of the symmetry, the locality of gates imposes no additional constraints.] We initialize the system and environment as

$$(\hat{\sigma}_\theta)_{se} = (\hat{\rho}_\theta)_s \otimes \hat{\pi}_e, \tag{69}$$

picking states that break the symmetry only on the system qubits and controlling the degree of symmetry breaking

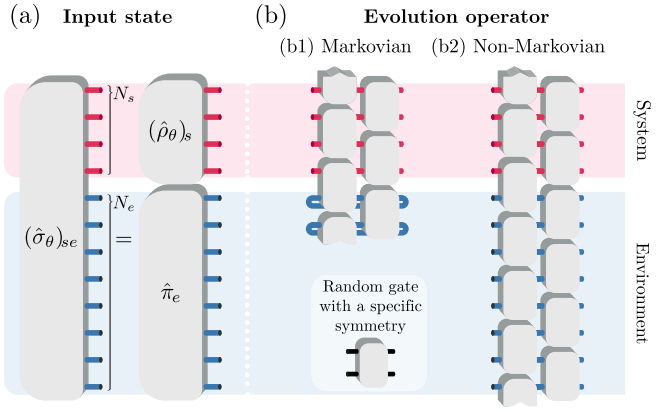

FIG. 8. Circuit schematics for the protocols in Sec. III G. (a) Preparation of the initial state: the system qubits (pink) are initialized in an asymmetric state parametrized by θ and the environment qubits in a symmetric state (blue). (b) Evolution operator: successive layers of two-qubit gates, each drawn at random subject to one of the two symmetry classes [U(1) and SU(2)], are arranged in a brickwork geometry. (b1) The Markovian channel is realized by resetting all environment qubits to the identity state after each $\hat{U}$ application. (b2) The non-Markovian channel is performed with no midcircuit reset or measurement, allowing information backflow from the environment to influence later evolution of the system.

through a tilt parameter θ, while $\hat{\pi}_e$ is a G-invariant state. This guarantees that the system evolution map

$$\mathcal{E}[\hat{\rho}_\theta] = \mathrm{Tr}_e[\hat{U}\hat{\sigma}_\theta\hat{U}^\dagger] \tag{70}$$

is a nonunitary CPTP which is G-covariant; namely, $\mathcal{E}$ is a free operation for the asymmetry resource (see Appendix G). At each time step, we compute the residual asymmetry with the relative entropy of asymmetry $M[\hat{\rho}_\theta(t)]$, as in Eq. (41).

1. Symmetry: U(1)

We now explore how U(1) symmetry (i.e., conservation of total $\hat{S}^z$) can give rise to a Mpemba effect in random circuits. In particular, we show how it is possible to achieve a strong Mpemba effect. Each two-qubit gate [100]

$$\hat{u}_{n,n+1} = e^{-i\hat{h}_{n,n+1}}e^{-ih_n\hat{s}^z_n}e^{-ih'_n\hat{s}^z_{n+1}} \tag{71}$$

combines an XXZ-type interaction

$$\hat{h}_{n,n+1} = \frac{J}{2}\left(\hat{s}^+_n\hat{s}^-_{n+1}e^{i\phi_n} + \hat{s}^-_n\hat{s}^+_{n+1}e^{-i\phi_n}\right) + J_z\hat{s}^z_n\hat{s}^z_{n+1} \tag{72}$$

with local z rotations $e^{-ih_n\hat{s}^z_n}$ and $e^{-ih'n\hat{s}^z_{n+1}}$. Here, $\hat{s}^\pm_n = \hat{s}^x_n \pm i\hat{s}^y_n$, and ϕ_n is the Peierls phase. By sampling the five parameters h_n, h'_n, ϕ_n, J, and J_z independently for each gate, the full circuit $\hat{U}$ remains U(1)-invariant, conserving total magnetization $\hat{S}^z$.

To study the Mpemba effect in circuits, we first discuss the clean Markovian limit with a memoryless environment and then generalize to non-Markovian circuits with a finite number of environment qubits. In the Markovian limit, the environment is reset after each layer, so that

$$\mathcal{E}_t = (\mathcal{E})^t, \qquad \mathcal{E} \equiv \mathcal{E}_1. \tag{73}$$

The environment state $\hat{\pi}_e$ is the maximally mixed state [see Fig. 8(b)]; each map $\mathcal{E}$ is U(1)-covariant [which guarantees monotonicity of $M[\hat{\rho}(t)]$] and, thus, decomposes into asymmetry sectors

$$\mathcal{E} = \bigoplus_\mu \mathcal{E}^{(\mu)}, \tag{74}$$

where $\mathcal{E}^{(\mu)}$ acts on the subspace of the operator space associated with mode μ. We can diagonalize each $\mathcal{E}^{(\mu)}$ individually using the basis $\{\hat{T}^{(\mu)}_\alpha\}$ as defined in Eq. (49) and obtain the decay eigenmodes in each μ sector.

To produce a strong Mpemba effect, we prepare product states of N_s qubits in blocks of size b with a uniform tilt θ:

$$|\varphi(\theta,b)\rangle = \bigotimes_{n=1}^{\lceil N_s/b\rceil} \exp\left[-i\theta\prod_{j=1}^{b}\hat{s}^y_{(n-1)b+j}\right]|0\rangle^{\otimes N_s}. \tag{75}$$

By varying θ and b, we select system states $\hat{\rho}_{\theta,b} = |\varphi(\theta,b)\rangle\langle\varphi(\theta,b)|$ whose support lies in different μ sectors (e.g., $b=1$ populates all μ sectors, $b=2$ populates only the even μ sectors, and $b=3$ only sectors multiple of 3, namely, $\hat{\rho}_{\theta,b} = \sum_{k=0}^{\lceil N_s/b\rceil-1}\hat{\rho}^{(kb)}_{\theta,b}$), so each state $\hat{\rho}_{\theta,b}$ overlaps differently with the slowest eigenmodes $\{\hat{\ell}_\mu\}_\mu$ [as in Fig. 9(d)] where

$$\hat{\ell}_\mu = \hat{\ell}_{k(\mu)}, \qquad \lambda_\mu = \lambda_{k(\mu)}, \tag{76}$$

where $k(\mu)$ picks out the slowest eigenmode in the μ sector

$$k(\mu) = \underset{k:\hat{\ell}_k\in\mathcal{B}(\mathscr{H}^{(\mu)}_s)}{\arg\max}\ \mathrm{Re}(\lambda_k), \tag{77}$$

where $\mathscr{H}^{(\mu)}_s$ is the μ sector of $\mathscr{H}_s$. The main panel in Fig. 9(a) then reveals distinct asymptotic decay exponents, i.e., a strong Mpemba effect. Avoiding overlap with specific μ sectors induces a strong Mpemba effect, because, in almost every realization of $\hat{U}$, sectors with larger $|\mu|$ decay more quickly: For $|\mu| > |\mu'|$, one finds $\mathrm{Re}(\lambda_\mu) < \mathrm{Re}(\lambda_{\mu'})$. Indeed, as illustrated in Fig. 9, the slowest eigenmodes reside in the blocks with the smallest $|\mu|$, that is, the lowest absolute U(1) charge. While a more thorough explanation of this phenomenon requires further investigation, one can consider the following possible mechanisms: (i) Modes with higher U(1) charge tend to

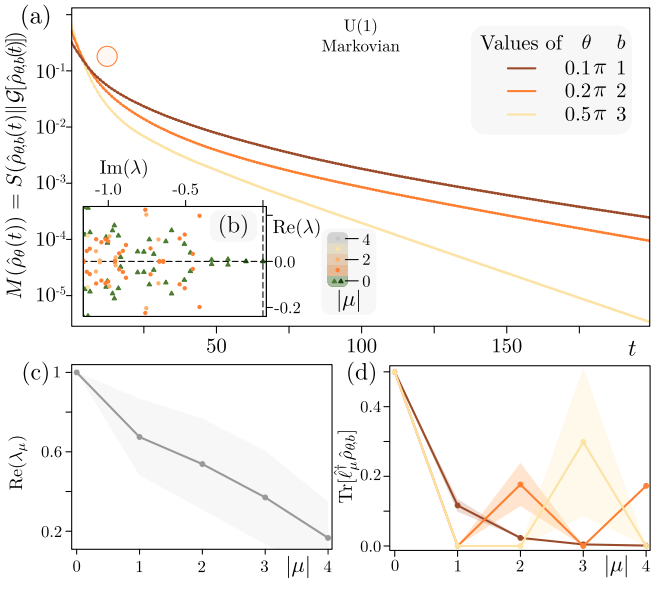

FIG. 9. Symmetry-breaking Mpemba effect in a Markovian U(1) model averaged over 100 circuit realizations with $N_s = 4$, $N_e = 2$. (a) shows the time evolution of the monotones. The inset (b) instead displays the averaged spectrum of the Markovian map, showing how the slow eigenmodes tend to come from low $|\mu|$ sectors, explaining the strong Mpemba effect ◯ obtained by choosing these three states. Mean (dots) and spread (shaded) of the real part of the slowest decay rate in each $|\mu|$ sector, showing a clear, monotonic decrease with $|\mu|$. It is evident that, as $|\mu|$ increases, $\mathrm{Re}(\lambda_\mu)$ decreases monotonically. (d) Overlap $\mathrm{Tr}[\hat{\ell}_\mu^\dagger \hat{\rho}_{\theta,b}]$ of each initial state with its sector's slowest eigenmode $\hat{\ell}_\mu$, confirming that each state couples only to sectors that are multiples of b.

evolve more rapidly, leading to faster buildup of correlations with the environment and, consequently, quicker information leakage and decay. (ii) Since $\mathcal{E}$ is constructed from random U(1)-conserving gates, the blocks corresponding to smaller $|\mu|$, being larger in dimension, are statistically more likely to contain the slowest-decaying eigenmodes. Moreover, just as in the example in Sec. III F, the initial state's overlap with the slow eigenmodes in sectors with $\mu \neq 0$ governs its relaxation rate. Note that the relative entropy of asymmetry $M[\hat{\rho}(t)]$ cannot be interpreted as entanglement asymmetry in this scenario, as the global state is not pure.

While the Markovian case allows for a clean explanation of the effect, most studies of the symmetry Mpemba effect use non-Markovian circuits. To connect to these, we again prepare a tilted product state on the system (with block size $b = 1$) with $\hat{\rho}_\theta = |\varphi(\theta)\rangle\langle\varphi(\theta)|$ and

$$|\varphi(\theta)\rangle = \bigotimes_{n=1}^{N_s} e^{-i\theta \hat{s}_n^y} |0\rangle_n \tag{78}$$

matching Refs. [33,73] except that the tilt now spans only the N_s system qubits, while the environment remains symmetric. Indeed, we initialize the environment in the computational zero state $\hat{\pi}_e = |0\rangle\langle 0_e| = |m_{\min}\rangle\langle m_{\min e}|$, where $|m\rangle$ denotes the equal superposition of all basis states with magnetization m and $\hat{s}_n^\alpha$ are the spin-$\frac{1}{2}$ operators (with $\alpha \in \{x, y, z\}$). Equation (74), which in the Markovian case describes how each symmetry-sector mode decays at a fixed rate, still applies when the map is non-Markovian. However, now it is time dependent, so both the eigenmodes and the stationary state can shift at each step, while the eigenvalues usually shrink exponentially with time when $\hat{U}$ is ergodic [101]. As already discussed, blocks with larger $|\mu|$ admit fewer eigenvalues near unity, so their modes decay more rapidly. Consequently, an initially highly asymmetric state, which has a larger weight in those fast-decaying, high-frequency sectors, will shed its asymmetry more quickly than a less asymmetric one, yielding the Mpemba effect. Figure 10 tracks five such states (different θ) on a system of $N_s = 8$ qubits coupled to $N_e = 12$ environment qubits.

Under general covariant time evolutions, asymmetry measures at time $t > 0$ are bounded by their value at $t = 0$, although in generic non-Markovian processes they can still exhibit transient increases at intermediate times. The deviations observed in Fig. 10 are, therefore, a consequence of information backflow [102] between the system and environment, amplified by the finite size of the environmental partition. We also emphasize that the monotonicity of asymmetry measures follows from the assumption that the environment is initially uncorrelated with the system and prepared in a symmetry-respecting state (see Appendix G). In contrast, initializing the environment in a symmetry-breaking state, e.g., tilted ferromagnetic states, as done in Refs. [72–74], violates this condition and can result in a non-G-covariant reduced map.

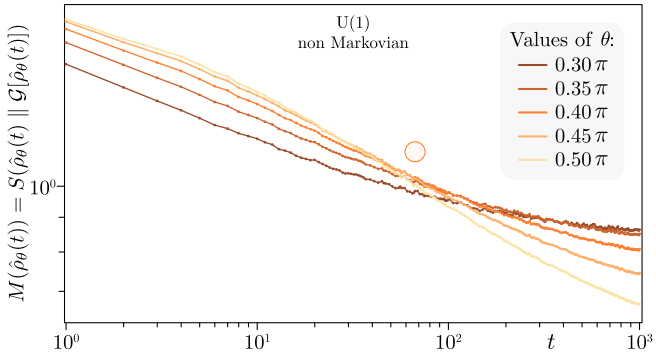

FIG. 10. Symmetry-breaking Mpemba effect in a non-Markovian U(1) model averaged over 100 circuit realizations with $N_s = 8$ and $N_e = 12$. The time evolution of the monotones reveals how the more tilted state, although it starts at a higher amount of asymmetry, restores the symmetry faster. Different from the Markovian case, the monotones do not decay either monotonically or exponentially, as the asymmetry is just distributed in the whole system + environment and, therefore, finite-size effects become more evident.

This distinction accounts for the apparent nonmonotonic behavior observed in non-Markovian circuit realizations of the U(1)-symmetric Mpemba effect.

In the examples shown in Figs. 9(c) and 9(d), we observe that sectors with larger $|\mu|$ tend to decay faster. We expect that a similar phenomenon holds more broadly beyond the Markovian case discussed here, including for random U(1)-invariant circuits with an arbitrary number of layers. A better understanding of this phenomenon requires further investigation. Our preliminary numerics on such circuits also suggest connections between the quasiparticle picture (Refs. [68,72]) and the mode-overlap picture, since one can directly compare overlaps with slow quasiparticle carriers and with slow asymmetric eigenmodes.

As a final note, these non-Markovian circuits closely mirror setups in deep thermalization with symmetries [103] and studies of dissipative quantum chaos [104].

2. *Symmetry: SU(2)*

We next turn to a non-Abelian example, where the conserved quantity is the total angular momentum $\hat{\mathbf{S}}^2$. To impose full SU(2) covariance, we switch off all local Z rotations and Peierls phases ($h_n = h'_n = \phi_n = 0$) and sample only the isotropic exchange coupling $J = J_z$.

We break the symmetry on the system by preparing the state $\hat{\rho}_\theta = |\varphi(\theta)\rangle\langle\varphi(\theta)|$ with

$$|\varphi(\theta)\rangle = \cos(\theta/2)|\xi\rangle^{\otimes\lfloor N_s/2\rfloor} + \sin(\theta/2)|0\rangle^{\otimes N_s}, \quad (79)$$

where $|\xi\rangle = (|01\rangle - |10\rangle)/\sqrt{2}$ is the singlet. For $\theta \neq k\pi \;\forall\; k \in \mathbb{Z}$, we find $|\varphi(\theta)\rangle$ in a superposition of the SU(2)-invariant singlet $|\xi\rangle^{\otimes\lfloor N_s/2\rfloor}$ and the SU(2)-breaking product $|0\rangle^{\otimes N_s}$. The environment, which contains an even number of qubits N_e, is also initialized in singlets, as $|\xi\rangle^{\otimes N_e/2}$. Note that, since the environment's state respects the SU(2) symmetry and the Hamiltonian also respects this symmetry, the dynamics of the reduced system likewise respects the symmetry; that is, it is SU(2)-covariant. [When the environment contains an odd number of qubits, it must be prepared in a mixed state in order to obtain an SU(2)-invariant state.]

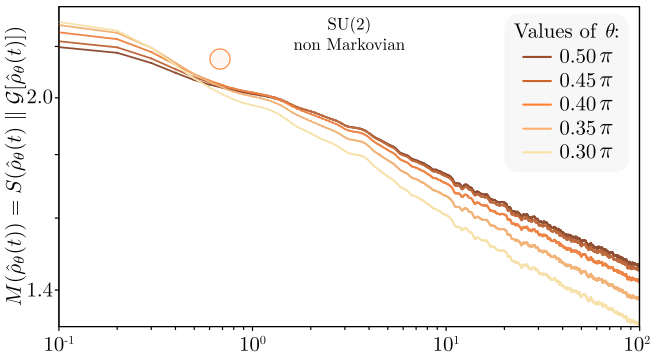

FIG. 11. Symmetry Mpemba effect for SU(2). The initial states are defined in Eq. (79), and we average over 100 random realizations of the dynamics generated by random SU(2)-symmetric gates with $N_s = 8$ and $N_e = 12$ drawing $J = J_z$ uniformly from $[-\pi/5, \pi/5]$ for each gate in $\hat{U}$.

Figure 11 shows five tilted states on an $N_s = 8$ system coupled to $N_e = 12$ environment qubits. As we vary θ, one can see characteristic crossings in their relaxation curves.

IV. A UNIFIED DESCRIPTION OF THE THERMAL AND THE SYMMETRY MPEMBA EFFECTS

We have reinterpreted instances of both the thermal (□) and symmetry (◯) Mpemba effects in systems interacting with featureless baths as well as in non-Markovian environments in a resource-theoretical approach in both classical and quantum settings. Strikingly, the mechanisms behind the thermal and symmetry Mpemba effects are remarkably similar: The former is governed by the slowest-decaying mode, while the latter relies on the slowest symmetry-restoring mode. Importantly, in both cases, the relevant monotone is based on the quantum relative entropy; what differs is the reference state with respect to which it is computed. For the thermal Mpemba effect □, it characterizes the divergence with respect to the steady state, while for the symmetry Mpemba effect ◯, it quantifies the divergence with respect to an instantaneously dephased state. It is well known that, for the Davies map, the relative entropy between a nonequilibrium state and the thermal steady state can be split into a classical and a purely quantum coherent part [105]. In this context, the system's Hamiltonian is the symmetry generator and, correspondingly, the twirling operation consists of dephasing the nonequilibrium state in the energy eigenbasis. Crucially, here we show that this approach can be generalized to an arbitrary symmetry as follows: Let G be a group with unitary representation $\{\hat{U}_g\}_{g\in\mathrm{G}}$ and $\mathcal{G}$ be the corresponding twirling map as in Eq. (35). For two states $\hat{\rho}, \hat{\pi}$ with $\mathcal{G}[\hat{\pi}] = \hat{\pi}$, the quantum relative entropy reads

$$\begin{aligned} S(\hat{\rho}\|\hat{\pi}) &= \mathrm{Tr}[\hat{\rho}\ln\hat{\rho}] - \mathrm{Tr}[\hat{\rho}\ln\hat{\pi}] \\ &\quad + \mathrm{Tr}[\hat{\rho}\ln\mathcal{G}[\hat{\rho}]] - \mathrm{Tr}[\hat{\rho}\ln\mathcal{G}[\hat{\rho}]] \\ &= S(\hat{\rho}\|\mathcal{G}[\hat{\rho}]) - \mathrm{Tr}[\hat{\rho}\ln\hat{\pi}] + \mathrm{Tr}[\hat{\rho}\ln\mathcal{G}[\hat{\rho}]]. \end{aligned} \quad (80)$$

Now, since $\hat{\pi}$ is G-invariant, we have that $\mathrm{Tr}[\hat{\rho}\ln\hat{\pi}] = \mathrm{Tr}[\hat{\rho}\ln\mathcal{G}[\hat{\pi}]]$. $\mathcal{G}\circ\mathcal{G} = \mathcal{G}$ and $\mathcal{G}^\dagger = \mathcal{G}$ imply

$$\mathrm{Tr}[\hat{\rho}\ln\mathcal{G}[\hat{\pi}]] = \mathrm{Tr}[\hat{\rho}\mathcal{G}[\ln(\mathcal{G}[\hat{\pi}])]] = \mathrm{Tr}[\mathcal{G}[\hat{\rho}]\ln\hat{\pi}]. \quad (81)$$

Analogously, we have that $\mathrm{Tr}[\hat{\rho}\ln\mathcal{G}[\hat{\rho}]] = \mathrm{Tr}[\mathcal{G}[\hat{\rho}]\ln\mathcal{G}[\hat{\rho}]]$. Hence, we find that

$$S(\hat{\rho}\|\hat{\pi}) = S(\hat{\rho}\|\mathcal{G}[\hat{\rho}]) + S(\mathcal{G}[\hat{\rho}]\|\hat{\pi}). \quad (82)$$

This equality holds for an arbitrary G-invariant state $\hat{\pi}$. In the special case where $\hat{\pi}$ is the thermal state, this identity

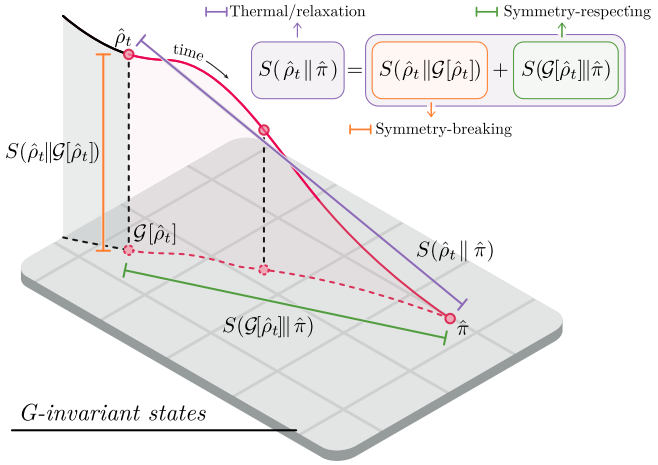

FIG. 12. Splitting of the relative entropy of athermality for systems exhibiting an arbitrary global symmetry into the relative entropy of asymmetry and the relative entropy of athermality for symmetry-respecting states. An initially asymmetric state $\hat{\rho}$ evolves under a G-covariant map toward the steady state that lies within the set of G-invariant states (see Sec. III A). The relative entropy of athermality of $\hat{\rho}(t)$ ($\hat{\rho}_t$ in the figure) (violet) can be split into two components: the relative entropy of $\hat{\rho}(t)$ with respect to the instantaneously dephased state $\mathcal{G}[\hat{\rho}(t)]$ (orange, namely, the relative entropy of asymmetry) and the relative entropy of $\mathcal{G}[\hat{\rho}(t)]$ with respect to $\hat{\pi}$ (green, namely, the relative entropy of athermality for symmetry-respecting states).

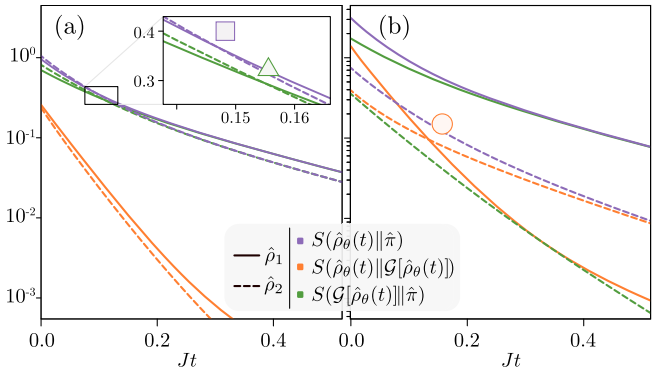

FIG. 13. Different Mpemba effects in the same thermalization process described by the Davies map. As in Fig. 7, we study a TFIM, setting $J = 1$, $h = 1$, $N_s = 4$, $\beta = 2$, and $\beta' = 1$ in both panels and initializing the system in the state $\hat{\rho}_1 = \hat{\rho}_{\text{Gibbs}}^{\text{rand}} = (\hat{\rho}_{\text{Gibbs}} + \gamma\hat{\rho}_{\text{rand}})/N$ and $\hat{\rho}_2 = \hat{R}_{\text{metr}}\hat{\rho}_1\hat{R}_{\text{metr}}^\dagger$ as in Sec. III F (full lines). The dashed lines are obtained by stochastically minimizing the overlap with the slowest-decaying mode via the Metropolis algorithm [26]. (a) For weak noise $\gamma = 0.05$, the dynamics display a classical thermal △ and a quantum thermal □ Mpemba effect. (b) For strong noise $\gamma = 0.25$, we find only the symmetry ○ Mpemba effect.

implies that the relative entropy of athermality can always be separated into the relative entropy of asymmetry (symmetry-breaking contribution) and the relative entropy of athermality for symmetry-respecting states (symmetry-respecting contribution), as illustrated in Fig. 12. We note that, by Eq. (22), in the special case where $\hat{\pi} = \hat{\pi}_\beta$ is the thermal state at temperature β^{-1}, the relative entropy $S(\hat{\rho}\|\hat{\pi}_\beta)$ can be expressed as the difference between the nonequilibrium free energy of $\hat{\rho}$ and that of $\hat{\pi}_\beta$. Furthermore, by Eq. (41), which was shown in Ref. [95], we have $S(\mathcal{G}[\hat{\rho}]\|\hat{\rho}) = S(\mathcal{G}[\hat{\rho}]) - S(\hat{\rho})$. Hence, in this special case, Eq. (82) simplifies to

$$F(\hat{\rho}) - F(\hat{\pi}_\beta) = \beta^{-1}[S(\mathcal{G}[\hat{\rho}]) - S(\hat{\rho})] + F(\mathcal{G}[\hat{\rho}]) - F(\hat{\pi}_\beta), \tag{83}$$

which was previously presented in Ref. [96].

This decomposition reveals that, for Davies maps, the quantum thermal Mpemba effect □ comprises a purely classical component △, corresponding to the classical thermal Mpemba effect, and a genuinely quantum part, which is associated with the restoration of time-translational symmetry generated by $\hat{H}_s$ ○. Here, as discussed in Ref. [26], eigenvalues associated with symmetry-preserving eigenmodes are real, while those corresponding to symmetry-breaking modes are complex (see Fig. 7). We stress that this distinction is not valid for more general G-covariant maps, as shown in Fig. 9. Moreover, there is nothing intrinsically quantum mechanical about the symmetry-breaking part of the dynamics. In fact, we showed a fully classical instance of a symmetry Mpemba effect in Sec. III D. So, in general, Eq. (82) decomposes the total athermality (or nonstationarity) monotone into two parts: the asymmetry monotone and a second part that quantifies the symmetry-respecting athermality [106].

As a final example, we study the occurrence of these different types of Mpemba effects in the same system. In Fig. 13, in both panels we consider the same thermalization process described by a Davies map but for different initializations of the state $\hat{\rho}_1$ as the Gibbs state with random noise defined in Eq. (66) with $\gamma = 0.05$ (a) and $\gamma = 0.25$ (b), while, as in Fig. 7, $\hat{\rho}_2 = \hat{R}_{\text{metr}}\hat{\rho}_1\hat{R}_{\text{metr}}^\dagger$. Here, the left panel shows both the classical and quantum thermal Mpemba effects, while the right panel displays only the symmetry Mpemba effect. While a crossing in either $S\{\hat{\rho}(t)\|\mathcal{G}[\hat{\rho}(t)]\}$ or $S\{\mathcal{G}[\hat{\rho}(t)]\|\hat{\pi}\}$ is necessary to induce a crossing in the total relative entropy $S[\hat{\rho}(t)\|\hat{\pi}]$, Eq. (82) implies that only when both component entropies cross are we guaranteed to find a crossing in $S[\hat{\rho}(t)\|\hat{\pi}]$. This example demonstrates that, in a given setting, one can seek different types of Mpemba effects, each connected to the depletion of a specific resource, by just changing the resource monotone M.

V. CONCLUSION

We have shown that the various manifestations of the Mpemba effect, arising from the restoration of thermal

equilibrium or symmetries, can all be cast within the unified framework of RTs. By formalizing each variant as a distinct resource-theoretic phenomenon, we clarified the conceptual boundaries between thermal Mpemba and symmetry Mpemba effects. Crucially, we demonstrated that it is not the specific physical embedding of the system (unitary versus featureless bath) that determines which Mpemba effect emerges but rather the choice of measure used to quantify the system's relaxation. Indeed, by selecting different resource measures, one can observe multiple Mpemba behaviors in the very same quantum model. Moreover, due to the absence of total ordering imposed by measures of resource in RTs, even when considering the same resource, the existence of the crossing characterizing the Mpemba effect depends on the considered monotone.

We highlighted how the quantum relative entropy has been used in studying the different Mpemba phenomena by taking as reference state the instantaneous projection of the state onto the free state set of the RT that corresponds to the Mpemba effect analyzed. This reveals a fundamental connection between the thermal Mpemba and the symmetry Mpemba effects. Crucially, the framework of the modes of asymmetry helps us extend the interpretation of thermal Mpemba effect to the symmetry one by shifting the attention of the initial overlap with the slowest-decaying mode to that with the slowest symmetry-breaking one, which dictates the timescale of the symmetry restoration. Following this approach, we identified the first instance of a symmetry Mpemba effect in a classical system. Moreover, we analyzed quantum symmetry Mpemba effects for global U(1) and SU(2) symmetries, considering both pure and mixed initial states.

The study of Mpemba effects within the framework of RTs reveals how different resources can dissipate at different rates, as illustrated in Fig. 13. Furthermore, given a RT with a Markovian free-evolution map $\mathcal{E}$, consider two initial states $\hat{\rho}_1$ and $\hat{\rho}_2$ with $M(\hat{\rho}_1) > M(\hat{\rho}_2)$. Let $\widehat{\ell}_j$ be the slowest-decaying resourceful eigenmode of $\mathcal{E}$ for which $\mathrm{Tr}[\widehat{\ell}_j^\dagger \hat{\rho}_2] \neq 0$. Then, $\hat{\rho}_1$ and $\hat{\rho}_2$ exhibit a Mpemba crossing:

$$M[\hat{\rho}_1(t)] < M[\hat{\rho}_2(t)] \quad \text{for some } t > 0, \tag{84}$$

if

$$|\mathrm{Tr}[\hat{\ell}_j^\dagger \hat{\rho}_1]| < |\mathrm{Tr}[\hat{\ell}_j^\dagger \hat{\rho}_2]|. \tag{85}$$

This provides a unified criterion for the occurrence of Mpemba-type behavior in any RT. By analyzing Mpemba dynamics, one can identify the mechanisms that cause certain resources to decay rapidly while others persist.

In this work, we have focused on quantum coherence, athermality, asymmetry, and nonstationarity (which in the classical context is particularly relevant for driven granular gases [9,13,14]), but this approach naturally extends to other resources such as entanglement, magic, and non-Gaussianity. Beyond unifying thermal and symmetry variants, this framework offers a principled route to designing protocols that accelerate or delay resource dissipation. Moreover, surveying diverse resource theories may uncover novel Mpemba-type phenomena in both classical and quantum domains. In this sense, resource theories provide conceptual structure within the ubiquitous but nonuniversal phenomenon that is the Mpemba effect.

ACKNOWLEDGMENTS

We thank Matteo Lostaglio, Felix Binder, Yutong Luo, Stephen Clark, Oisín Culhane, and Sara Murciano for discussions. This work was supported by the EPSRC-Research Ireland joint project QuamNESS and by Research Ireland under the Frontier For the Future Program. J. G. is supported by a Research Ireland Royal Society University Research Fellowship. A. S. acknowledges the financial support provided by Microsoft Ireland. M. M. acknowledges funding from the Royal Society and Research Ireland. X. T. acknowledges DFG Collaborative Research Center (CRC) 183 Project No. 277101999, project B01 and DFG under Germany's Excellence Strategy—Cluster of Excellence Matter and Light for Quantum Computing (ML4Q) EXC 2004/1-390534769. I. M. acknowledges support from NSF Phy-2046195, NSF FET-2106448, and NSF QLCI Grant No. OMA-2120757.

DATA AVAILABILITY

The data that support the findings of this article are openly available [107].

APPENDIX A: NONTHERMAL MPEMBA EFFECT AND THE RESOURCE THEORY OF NONSTATIONARITY

In the following, we address Mpemba effects in the pure relaxation dynamics of open quantum systems. We consider states $\hat{\rho}(t)$ evolving under Markovian and time-homogeneous Lindblad dynamics. We assume that the Liouvillian has a unique, full-rank steady state $\hat{\pi}$ to which any state converges in the long-time limit. The solution to the Lindblad master equation defines a one-parameter semigroup of CPTP maps

$$\mathcal{E}_t = e^{t\mathcal{L}}, \qquad t \geq 0. \tag{A1}$$

We demonstrate that pure relaxation Mpemba effects are captured within the resource theory of nonstationarity, inspired by the resource theory of athermality [51]. The free states in this framework are steady states $\hat{\pi}$, while any other state is considered resourceful. Free operations $\mathcal{E}$ must satisfy

(1) preservation of the steady state: $\mathcal{E}[\hat{\pi}] = \hat{\pi}$;

(2) phase covariance: $\mathcal{U}_t \circ \mathcal{E} = \mathcal{E} \circ \mathcal{U}_t$, where $\mathcal{U}_t$ is given by

$$\mathcal{U}_t[\cdot] = \hat{\pi}^{it}[\cdot]\hat{\pi}^{-it}, \tag{A2}$$

for arbitrary $t \in \mathbb{R}$.

Interestingly, and generalizing the result on thermalizing maps that connects the athermality monotone to the nonequilibrium free energy, the monotone of nonstationarity, $S[\hat{\rho}(t)\|\hat{\pi}]$, is also connected to a known thermodynamic quantity, namely, the nonadiabatic entropy production [108] for a full relaxation from $\hat{\rho}(t) \to \hat{\pi}$:

$$\Sigma_{\mathrm{na}}(t) = M[\hat{\rho}(t)] = S[\hat{\rho}(t)\|\hat{\pi}]. \tag{A3}$$

Note that, if the fixed point is thermal, the above recovers the total entropy production as originally introduced by Spohn [109].

As an example, we consider an all-to-all spin model, akin to laser-driven interacting ensembles of Rydberg atoms [24,110–112], to demonstrate the Mpemba effect in an open quantum system with a nonthermal fixed point. This model has been studied in the context of the quantum Mpemba effect in Ref. [20]. In adopting their description, we model N_s atoms as two-level systems, described collectively with the spin operators $\hat{S}_\alpha$ and total angular momentum j^2. For simplicity, we consider the symmetry sector, for which $j^2 = N_s(N_s+2)/4$. Its basis is formed by the eigenstates of the $\hat{S}_z$ operator, $\hat{S}_z|m\rangle = m|m\rangle$, with m running from $m = -N_s/2$ to $m = N_s/2$. The Hamiltonian is given by

$$\hat{H} = \Omega\hat{S}_x - \Delta\hat{S}_z + \frac{V}{N_s}\hat{S}_z^2, \qquad \hat{L} = \sqrt{\kappa}\hat{S}_-. \tag{A4}$$

Here, $\hat{S}_- = \hat{S}_x - i\hat{S}_y$, Ω is the Rabi frequency, Δ is the laser detuning from the atomic frequency, and V denotes the strength of the all-to-all interactions. We choose initial states $\hat{\rho}_1$ and $\hat{\rho}_2$ such that $S(\hat{\rho}_2\|\hat{\pi}) > S(\hat{\rho}_1\|\hat{\pi})$. As the states evolve under the dynamics generated by the Lindblad master equation specified by the Hamiltonian and jump operator in Eq. (A4), we observe a Mpemba effect ☆ in the relative entropy with respect to $\hat{\pi}$, serving as a monotone for the resource of nonstationarity, shown in Fig. 14. Finally, we note that the resource of nonstationarity and its associated monotone may also be relevant for certain classical systems. In particular, granular gases have been shown to exhibit Mpemba effects, e.g., Refs. [9,13,14]. In regimes where the single-particle dynamics are approximately linear and admit a unique steady state, such systems could potentially be described within a similar framework, with the Kullback-Leibler divergence serving as the nonstationarity monotone. While extending this perspective to more complex or strongly nonlinear granular gases may not be straightforward, these systems offer an interesting direction for future investigations of Mpemba effects in classical settings.

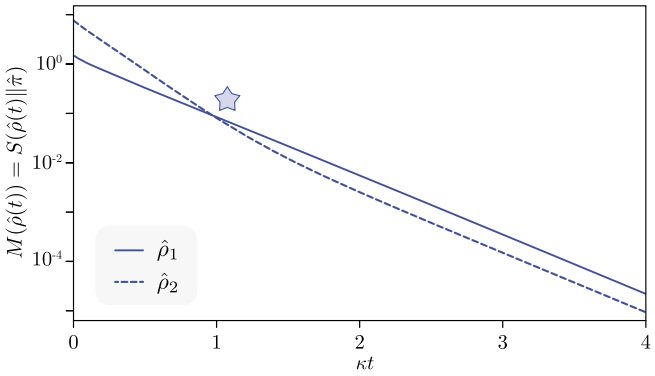

FIG. 14. Quantum Mpemba effect in a pure relaxation process of an all-to-all spin model. The monotone quantifying the resource of nonstationarity is the relative entropy between the time-evolved initial states and the fixed point $\hat{\pi}$. Parameters: $N_s = 5$, $\Omega = 1$, $\Delta = -1$, $V = 3$, and $\kappa = 0.01$.

APPENDIX B: THERMAL MPEMBA EFFECT WITH ETH

In the literature, the thermal Mpemba effect has been explored mainly in Markovian open quantum systems obeying Eq. (19), with the recent exception of Ref. [113], where it was also found in isolated systems. Here, we show that this effect can be found also in a subpart of a quantum system evolving unitarily. A single qubit, when weakly coupled to a nonintegrable environment satisfying the ETH [114,115], relaxes to a thermal state whose temperature is determined by the total initial energy of the qubit plus environment. Following Ref. [116], we consider the total Hamiltonian

$$\hat{H}_{\mathrm{se}} = \hat{H}_s + \hat{V} + \hat{H}_e, \tag{B1}$$

with

$$\hat{H}_s = h_0\hat{s}_0^z, \qquad \hat{V} = \kappa\hat{s}_0^x \otimes \hat{s}_1^x, \tag{B2}$$

where ω_0 is the system qubit's frequency and κ denotes the system-environment coupling. The environment Hamiltonian is

$$\hat{H}_e = J_z\sum_{n=1}^{N-1}\hat{s}_n^z\hat{s}_{n+1}^z + h_1\hat{s}_1^z + h_N\hat{s}_N^z + \sum_{n=1}^{N} h_z\hat{s}_n^z + h_x\hat{s}_n^x. \tag{B3}$$

We choose initial states of the form

$$|\psi_\theta\rangle_{se} = |\varphi_\theta\rangle_s \otimes |E_\theta\rangle_e \tag{B4}$$

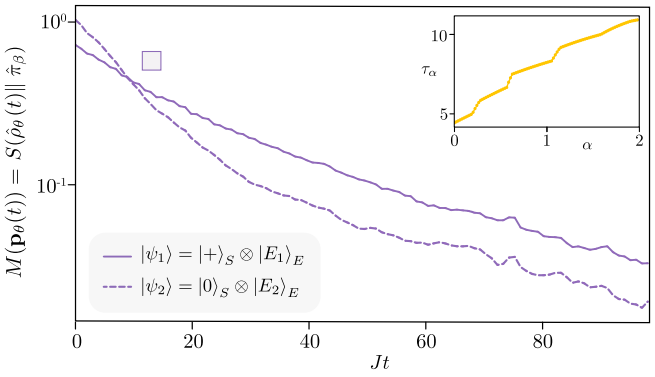

FIG. 15. Quantum thermal Mpemba effects in a subpart of a system evolving unitarily. We considered the Hamiltonian Eq. (B1) with $(J, h_z, h_x, h_1, h_N, \kappa, h_0) = (1, 0.3, 1.1, 0.25, -0.25, 0.15, 1.525)$, $\beta = -0.46$, and $N = 15$. Inset: the crossing times τ_α obtained by studying the different α divergence [see Eq. (3)].

with $\theta = 1,\ 2$, $|\varphi_1\rangle = |+\rangle$, and $|\varphi_2\rangle = |0\rangle$. $|E_\theta\rangle$ is an eigenstate of $\hat{H}_e$ chosen so that the inverse temperature β of the overall state (that is fixed by the energy of $|\psi_\theta\rangle_{se}$) matches. This, together with ETH, ensures that the two different initial states on s converge to the same thermal steady state $\hat{\pi}_\beta = e^{-\beta\hat{H}_s}/\mathrm{Tr}[-\beta\hat{H}_s]$, within the fluctuations anticipated by ETH.

The evolution of the system's state is described by a CPTP map

$$\begin{aligned}\hat{\rho}_\theta(t) &= \mathcal{E}_t[\hat{\rho}_\theta] \\ &= \mathrm{Tr}_e[e^{-it\hat{H}_{se}}(|\varphi_\theta\rangle\langle\varphi_\theta| \otimes |E_\theta\rangle\langle E_\theta|)e^{it\hat{H}_{se}}]. \end{aligned} \tag{B5}$$

To quantify the divergence of $\hat{\rho}_\theta(t)$ with respect to $\hat{\pi}_\beta$, we employ the monotone of Eq. (8). As the map is not Markovian, $M[\hat{\rho}_\theta(t)]$ is guaranteed to be monotonic only between time 0 and $t > 0$. At intermediate times, we note small fluctuations which eventually can be considered as finite-size effects which would vanish completely when considering an infinitely large bath, for which the map $\mathcal{E}_t$ becomes Markovian [117]. Figure 15 shows the crossing of the relative entropies indicating the occurrence of a quantum thermal Mpemba effect □. The inset shows that, when using α divergences, the crossing time τ_α depends on α.

APPENDIX C: ASYMPTOTIC DECAY OF THE QUANTUM RELATIVE ENTROPY

For both classical and quantum systems, the late time behavior of a state is determined by its overlap with the slowest-decaying eigenmode, among the whole spectrum for athermality and only among the nonzero-μ sectors for asymmetry. Here, we prove Eqs. (17) and (24).

1. Proof of the asymptotic decay of the KL divergence

Let $\hat{\mathcal{L}}^{\mathrm{cl}}$ be a classical Liouvillian obeying detailed balance, with unique stationary distribution $\boldsymbol{\pi}$, which we assume has full support ($\pi_i > 0$ for all i). Let us define the weighted inner product

$$\langle \mathbf{u}, \mathbf{v}\rangle_{\boldsymbol{\pi}} = \sum_i \frac{u_i v_i}{\pi_i}, \tag{C1}$$

and let us order the eigenvalues of $\hat{\mathcal{L}}^{\mathrm{cl}}$ as

$$0 = \lambda_1 > \lambda_2 \geq \lambda_3 \geq \cdots. \tag{C2}$$

We further assume the spectrum to not be degenerate for λ_j, with $j = 2$ in the case of athermality (see Sec. II) and j corresponding to the slowest asymmetric eigenmode for asymmetry (see Sec. III). Denoting the corresponding eigenmodes by $\mathbf{r_k}$ (orthonormal under $\langle\cdot,\cdot\rangle_{\boldsymbol{\pi}}$),

$$\hat{\mathcal{L}}^{\mathrm{cl}}\mathbf{r}_k = \lambda_k \mathbf{r}_k, \qquad \langle \mathbf{r}_k, \mathbf{r}_\ell\rangle_{\boldsymbol{\pi}} = \delta_{k\ell}. \tag{C3}$$

In this eigenbasis, an initial probability distribution $\mathbf{p}$ evolves as

$$\mathbf{p}(t) = \boldsymbol{\pi} + \sum_{k\geq 2} a_k \mathbf{r}_k e^{\lambda_k t}, \qquad a_k = \langle \mathbf{p}, \mathbf{r}_k\rangle_{\boldsymbol{\pi}}, \tag{C4}$$

so that $\delta\mathbf{p}(t) = \mathbf{p}(t) - \boldsymbol{\pi} = \sum_{k\geq 2} a_k \mathbf{r}_k e^{\lambda_k t}$. For small deviations, one finds

$$D[\mathbf{p}(t)\|\boldsymbol{\pi}] = \sum_k p_k(t) \ln\frac{p_k(t)}{\pi_k} \sim \frac{1}{2}\sum_k \frac{[\delta p_k(t)]^2}{\pi_k}. \tag{C5}$$

As $t \to \infty$, as noted in Ref. [118], only the slowest-decaying mode ($j = 2$) survives, $\delta p_k \sim a_2 r_{2,k} e^{\lambda_2 t}$, giving Eq. (17)

$$D[\mathbf{p}(t)\|\boldsymbol{\pi}] \sim \frac{1}{2} a_2^2 e^{2\mathrm{Re}(\lambda_2)t} \sum_k \frac{r_{2,k}^2}{\pi_k}.$$

Replacing $\boldsymbol{\pi}$ with $\hat{\mathcal{G}}\mathbf{p}(t)$ allows one to extend this to the asymptotic behavior of the relative entropy of asymmetry.

2. Proof of the asymptotic decay of the quantum relative entropy

In both the thermalization example in Sec. II C and the symmetry-breaking scenario in Sec. III, our main monotone

$$M[\hat{\rho}(t)] = S[\hat{\rho}(t)\|\hat{\pi}_\beta] \quad \text{or} \quad S\{\hat{\rho}(t)\|\mathcal{G}[\hat{\rho}(t)]\} \tag{C6}$$

is the quantum relative entropy between the evolving state and its target (the relative entropy of athermality and of asymmetry, respectively). At long times, its decay is governed by the slowest eigenmode of the Lindbladian $\mathcal{L}$

having nonzero overlap with the initial state, following Eq. (24) for the thermal Mpemba effect and Eq. (58) (in the case of the $\mathbb{Z}_4$ example studied in Sec. III D) for the asymmetry Mpemba effect.

Let now $\mathcal{L}$ be diagonalizable. Then, there exist right eigenmodes $\{\hat{r}_k\}$ and left eigenmodes $\{\hat{\ell}_k\}$ satisfying

$$\mathcal{L}[\hat{r}_k] = \lambda_k \hat{r}_k, \qquad \mathcal{L}^\dagger[\hat{\ell}_k] = \lambda_k^* \hat{\ell}_k, \tag{C7}$$

with the biorthonormality condition

$$\mathrm{Tr}[\hat{\ell}_k^\dagger \hat{r}_\ell] = \delta_{k\ell} \tag{C8}$$

and corresponding spectrum ordered so that

$$0 = \mathrm{Re}(\lambda_1) > \mathrm{Re}(\lambda_2) \geq \mathrm{Re}(\lambda_3) \geq \cdots. \tag{C9}$$

As in Appendix C 1, we also assume the slowest eigenmode associated to eigenvalue λ_j to be nondegenerate (for athermality, $j = 1$; for asymmetry, the index j is chosen among eigenmodes in $\mu \neq 0$ sectors as in the main text).

We now sketch the proof in three steps.

(I) *Spectral expansion*: Analogously to Eq. (C4), any initial state decomposes as

$$\hat{\rho}(t) = \hat{\pi} + \sum_{k\geq 2} c_k \hat{r}_k e^{\lambda_k t}, \qquad c_k = \mathrm{Tr}[\hat{\ell}_k^\dagger \hat{\rho}]. \tag{C10}$$

(II) *Quadratic approximation of S*: Writing $\hat{\rho} = \hat{\pi} + \delta\hat{\rho}$ with $\|\delta\hat{\rho}\| \ll 1$, one shows via the integral representation of the logarithm that

$$S(\hat{\rho}\|\hat{\pi}) = \mathrm{Tr}[\hat{\rho}(\ln\hat{\rho} - \ln\hat{\pi})] \approx \frac{1}{2}\mathrm{Tr}[\delta\hat{\rho}\hat{\pi}^{-1}\delta\hat{\rho}]. \tag{C11}$$

(III) *Dominance of the slowest eigenmode*: At late times, $\delta\hat{\rho}(t) \approx c_j \hat{r}_j e^{\lambda_j t}$. If $\lambda_j \in \mathbb{C}\backslash\mathbb{R}$, its conjugate partner λ_j^* must also be included, and one finds

$$\delta\hat{\rho}(t) \approx c_j \hat{r}_j e^{\lambda_j t} + c_j^* \hat{r}_j^\dagger e^{\lambda_j^* t}. \tag{C12}$$

Substituting into Eq. (C11) gives

$$\mathrm{Tr}[\delta\hat{\rho}\hat{\pi}^{-1}\delta\hat{\rho}] \approx \begin{cases} |c_j|^2 e^{2\mathrm{Re}(\lambda_j)t}\mathrm{Tr}[\hat{r}_j^\dagger \hat{\pi}^{-1}\hat{r}_j], & \lambda_j \in \mathbb{R}, \\ 2|c_j|^2 e^{2\mathrm{Re}(\lambda_j)t}\mathrm{Re}(\mathrm{Tr}[\hat{r}_j^\dagger \hat{\pi}^{-1}\hat{r}_j]), & \lambda_j \notin \mathbb{R}. \end{cases} \tag{C13}$$

Hence,

$$S(\hat{\rho}(t)\|\hat{\pi}) \sim \begin{cases} \frac{1}{2}|c_j|^2 e^{2\mathrm{Re}(\lambda_j)t}\mathrm{Tr}[\hat{r}_j^\dagger \hat{\pi}^{-1}\hat{r}_j], & \lambda_j \in \mathbb{R}, \\ |c_j|^2 e^{2\mathrm{Re}(\lambda_j)t}\mathrm{Re}(\mathrm{Tr}[\hat{r}_j^\dagger \hat{\pi}^{-1}\hat{r}_j]), & \lambda_j \notin \mathbb{R}, \end{cases} \tag{C14}$$

as discussed in Ref. [119]. Note that this can be straightforwardly extended to $S(\hat{\rho}(t)\|\mathcal{G}[\hat{\rho}(t)])$ by replacing $\hat{\pi}$ with $\mathcal{G}[\hat{\rho}(t)]$ in the proof.

APPENDIX D: MONOTONE-DEPENDENT OCCURRENCE OF THE MPEMBA CROSSING

In Figs. 2 and 3 in the main text, we examined the thermal Mpemba effect in a classical and a quantum Markovian setting, respectively. The crossing time τ_α, defined as the point where the two M_α curves intersect, was found to vary smoothly with the monotone parameter α. As defined in the main text, these monotones correspond to the classical and quantum Rényi relative entropies M_α between the time-evolved states and the equilibrium steady states. Here, we demonstrate that this dependence of the crossing times on the monotones implies that one can find pairs of states and two parameters α_1 and α_2 such that a Mpemba crossing appears for $M_{\alpha_1}(t)$ but not for $M_{\alpha_2}(t)$. This dependence implies that one can find pairs of states and two parameters α_1 and α_2 such that a Mpemba crossing appears for $M_{\alpha_1}(t)$ but not for $M_{\alpha_2}(t)$. Since, at least within a certain range, τ_α increases monotonically with α, we can choose the initial states as time-evolved states at a time t^* satisfying $\tau_{\alpha_1} < t^* < \tau_{\alpha_2}$. Consequently, for α_1 the crossing time lies earlier along the forward time axis than t^*, whereas for α_2 it lies later. Because the dynamics are irreversible and backward histories are not unique, "earlier" and "later" should be understood with respect to forward evolution from the chosen preparatory

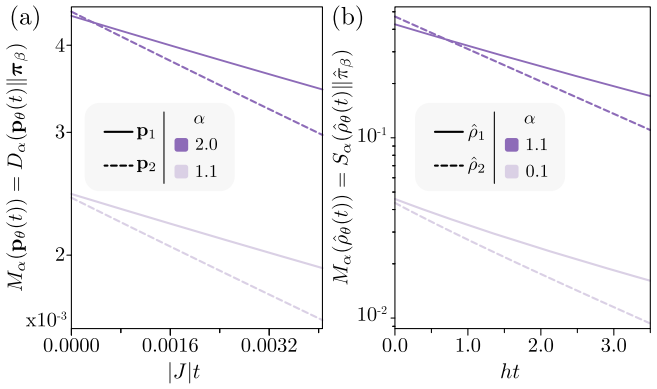

FIG. 16. The presence or absence of the Mpemba crossing depends on the chosen monotone. (a) Classical case: we initialize the system with the time-evolved thermal state (full lines) and optimized state (dashed lines) from Fig. 2 at time $|J|t^* \approx 0.376$. We compute the classical Rényi relative entropy Eq. (18) between the time-evolved states and the equilibrium steady state for $\alpha = 1.1$ (lighter lines) and $\alpha = 2$ (opaque lines). In (b), we initialize the system with the time-evolved random state (full lines) and optimized state (dashed lines) from Fig. 3 at time $ht^* \approx 2$. We show the quantum Rényi relative entropy Eq. (7) between the time-evolved states and the equilibrium steady state for $\alpha = 0.1$ (lighter lines) and $\alpha = 1.1$ (opaque lines).

procedure (the states obtained at t^*) rather than as uniquely defined backward trajectories.

We illustrate this behavior in Fig. 16, where Fig. 16(a) shows a classical example and Fig. 16(b) shows a quantum one. For the classical case, we take as initial states the pair of configurations considered in Fig. 2 at time $t^* \approx 0.94$, while for the quantum case we initialize the dynamics with the two states from Fig. 3 at time $t^* \approx 0.20$. This illustrates that, at least when nonequilibrium initial states are allowed, the occurrence of a Mpemba crossing depends on the chosen monotone function used to characterize it, even when these monotones quantify the same resource (athermality, in this case).

APPENDIX E: DETAILS ON THE DAVIES MAP

The Davies map arises from a particular Lindblad equation describing the thermalization of quantum systems weakly coupled to a Markovian heat bath [59]. In the main text, we have focused on its general mathematical properties, while here we give the explicit expression of the equation that we used to compute various examples. Consider the spectral decomposition of the system's Hamiltonian $\hat{H}_s = \sum_k h_k |k\rangle\langle k|$. In the eigenbasis of $\hat{H}_s$, the Davies generator reads

$$\frac{d\hat{\rho}_s(t)}{dt} = \mathcal{L}[\hat{\rho}_s(t)] = -i[\hat{H}_s, \hat{\rho}_s(t)] + \sum_{k<k'} \mathcal{D}^{(1)}_{kk'}[\hat{\rho}_s(t)] + \mathcal{D}^{(2)}_{kk'}[\hat{\rho}_s(t)], \tag{E1}$$

where the dissipators $\mathcal{D}^{(1)}_{kk'}$ and $\mathcal{D}^{(2)}_{kk'}$ are generated by the jump operators $\hat{L}^{(1)}_{kk'}$ and $\hat{L}^{(2)}_{kk'}$, respectively, which couple all Hamiltonian eigenstates as

$$\hat{L}^{(1)}_{kk'}(\beta) = [1 \mp f^{\pm}(\beta, h_{k'} - h_k)]^{1/2} |k\rangle\langle k'|,$$
$$\hat{L}^{(2)}_{kk'}(\beta) = [f^{\pm}(\beta, h_{k'} - h_k)]^{1/2} |k'\rangle\langle k'|. \tag{E2}$$

Here, $f^{\pm}(\beta, h_{k'} - h_k) = 1/\{\exp[\beta(h_{k'} - h_k)] \pm 1\}$ are the Fermi (+) and the Bose (−) distribution functions which enforce the detailed balance condition, ensuring that the unique steady state is the thermal state at inverse temperature β. Throughout all examples in the main text, we considered bosonic canonical commutation relations.

APPENDIX F: QUANTUM FISHER INFORMATION AND WHY THE MEASURE MATTERS

Let us assume that the dynamics of a system described by the state $\hat{\rho}$ are Markovian and that the state evolves according to

$$\frac{d\hat{\rho}}{dt} = \mathcal{L}[\hat{\rho}], \tag{F1}$$

where $\mathcal{L}$ is the generator of the dynamics and takes the Lindblad form. Following Ref. [65], we define the symmetries of the Lindbladian as the set of superoperators that commute with $\mathcal{L}$:

$$\mathrm{Sym}(\mathcal{L}) := \{\mathcal{M} \in \mathscr{B}[\mathscr{B}(\mathscr{H})] | [\mathcal{M}, \mathcal{L}] = 0\}, \tag{F2}$$

where $\mathscr{B}[\mathscr{B}(\mathscr{H})]$ denotes the set of bounded linear operators acting on the space of bounded linear operators on the finite-dimensional Hilbert space $\mathscr{H}$.

Here, we focus on the special case where the symmetry superoperator is the Lindbladian itself, i.e., $\mathcal{M} = \mathcal{L}$. In this case, any quantum Fisher information with respect to the time parameter serves as a monotone under the evolution generated by $\mathcal{L}$. The family of QFI about the time parameter t can be written in the form

$$I_f(t) = \sum_{x,y} \frac{|\langle x(t)|\mathcal{L}[\hat{\rho}_t]|y(t)\rangle|^2}{p_x(t) f[p_y(t)/p_x(t)]}, \tag{F3}$$

where the density matrix is expressed in its spectral decomposition $\hat{\rho} = \sum_x p_x |x\rangle\langle x|$. The set $\{p_x\}$ defines a discrete probability distribution over eigenstates. The function f characterizes the particular QFI measure within the family and is required to satisfy three properties, (i) operator monotonicity: for any positive semidefinite operators A and B such that $A \leq B$, it holds that $f(A) \leq f(B)$; (ii) self-inversiveness: $f(x) = xf(1/x)$ for all $x > 0$; (iii) normalization: $f(1) = 1$.

Common examples of such QFI measures include the symmetric logarithmic derivative (SLD) QFI with $f_{\mathrm{SLD}}(x) = [(x+1)/2]$, which is minimal in this family, the Wigner-Yanase (WY) QFI with $f_{\mathrm{WY}}(x) = \frac{1}{4}(\sqrt{x}+1)^2$, and the harmonic mean (HM) QFI with $f_{\mathrm{HM}}(x) = [2x/(x+1)]$, which is the maximal element in this class.

For a more detailed discussion of these QFI families and their properties, see Ref. [66].

As discussed in Ref. [65], this perspective can be naturally integrated into the framework of quantum resource theories, particularly those in which the free operations are generated by the dynamical map $\mathcal{E}_t := \exp(t\mathcal{L})$. In such a setting, the resource is identified with the degree of nonstationarity, as previously defined.

It is crucial to emphasize, however, that monotones associated with a given symmetry $\mathcal{M}$ do not, in general, induce a total order on quantum states. Specifically, if a monotone M_a satisfies $M_a(\hat{\rho}_1) > M_a(\hat{\rho}_2)$ for two states $\hat{\rho}_1$ and $\hat{\rho}_2$, this does not necessarily imply that another monotone M_b associated with the same symmetry will also yield $M_b(\hat{\rho}_1) > M_b(\hat{\rho}_2)$. In fact, we present an explicit

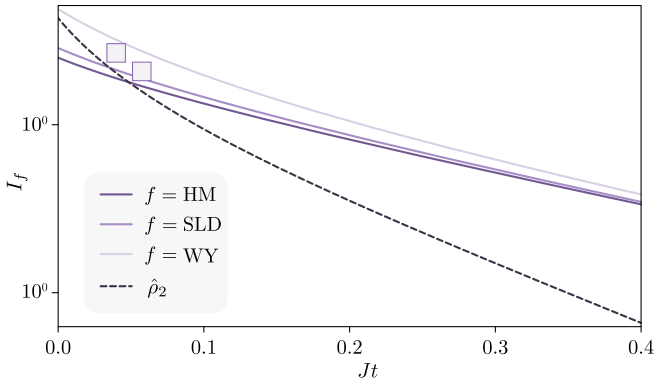

FIG. 17. Quantum Fisher information I_f for different monotones during the thermal relaxation of a single qubit. The initial states are unitarily connected, with one being incoherent (dashed line) and the other coherent (full lines) in the energy eigenbasis. Because of the structure of the Davies generator, the incoherent state's dynamics and corresponding I_f are independent of the choice of f, while the coherent state's behavior depends strongly on the monotone. The SLD and WY monotones both exhibit an Mpemba crossing at distinct times, whereas the HM monotone does not display a crossing. Parameters: $(r_x, r_y, r_z) = (0.75, 0, 0.19)$, $J = 1$, $\beta = 0.1\ \mathrm{J}^{-1}$, $\gamma = 1J$, and $\omega = 5J$.

counterexample illustrating this point. Moreover, we explore the consequences of this monotone dependence in the context of crossing times, particularly as it pertains to (quantum) Mpemba behavior.

To this end, we revisit the thermal quantum Mpemba effect that emerges in the pure relaxation dynamics of a single qubit coupled to a thermal bath, as discussed in Sec. II C in the main text. We consider the relaxation behavior of two distinct, but unitarily connected, initial states: one of which is coherent in the energy eigenbasis, while the other ($\hat{\rho}_2$) is not. Owing to the structure of the Davies generator, the evolution of populations and coherences in the energy basis decouples. Furthermore, the quantity I_f naturally splits into two contributions: one incoherent and one coherent, defined with respect to the instantaneous eigenbasis of the state.

Given these two facts, it is straightforward to see that, for the incoherent state, only the incoherent component contributes to I_f. Importantly, this contribution is independent of the choice of the function f, as illustrated by the dashed gray line in Fig. 17. In contrast, the initially coherent state yields an f-dependent contribution, as shown by the colored lines in Fig. 17. Notably, the monotones I_{SLD} and I_{WY} exhibit a Mpemba crossing, though at distinct crossing times, while I_{HM} does not show any crossing. This demonstrates that both the presence of an Mpemba crossing and the associated crossing time are strongly dependent on the specific choice of monotone, even when the underlying resource is held fixed.

APPENDIX G: FROM GLOBAL G INVARIANCE TO LOCAL G COVARIANCE

In this section, we demonstrate how a global symmetry of a joint system-environment unitary evolution induces covariance of the reduced system dynamics under the same symmetry group, if the environment is prepared in a symmetric state. Let us consider a G group, $\hat{T} \in \mathscr{B}(\mathscr{H}_s \otimes \mathscr{H}_e)$ a G-invariant unitary, and $\hat{\pi}_e \in \mathscr{S}(\mathscr{H}_e)$ a G-invariant state. Then, the map

$$\mathcal{E}[\cdot] = \mathrm{Tr}_e[\hat{T}([\cdot] \otimes \hat{\pi}_e)\hat{T}^\dagger] \tag{G1}$$

will be G-covariant, namely,

$$\mathcal{E}[\hat{U}_{g,s}\hat{\rho}\hat{U}_{g,s}^\dagger] = \hat{U}_{g,s}\mathcal{E}[\hat{\rho}]\hat{U}_{g,s}^\dagger \quad \forall\ \hat{\rho} \in \mathscr{S}(\mathscr{H}_s), \tag{G2}$$

where $\hat{U}_{g,s}$ is the unitary representation of G on $\mathscr{H}_s$.

To prove this, let us consider a unitary representation of the group $\hat{U}_g = \hat{U}_{g,s} \otimes \hat{U}_{g,e}$ on $\mathscr{H}_s \otimes \mathscr{H}_e$ and begin from the left-hand side:

$$\mathcal{E}[\hat{U}_{g,s}\hat{\rho}\hat{U}_{g,s}^\dagger] = \mathrm{Tr}_e[\hat{T}(\hat{U}_{g,s}\hat{\rho}\hat{U}_{g,s}^\dagger \otimes \hat{\pi})\hat{T}^\dagger]. \tag{G3}$$

By G invariance we have $[\hat{T}, \hat{U}_{g,s} \otimes \hat{U}_{g,e}] = 0\ \ \forall\ \ g \in \mathrm{G}$, so

$$\hat{T}(\hat{U}_{g,s}\hat{\rho}\hat{U}_{g,s}^\dagger \otimes \hat{\pi})T^\dagger = \hat{U}_{g,s} \otimes \hat{U}_{g,e}(\hat{\sigma})\hat{U}_{g,s}^\dagger \otimes \hat{U}_{g,e}^\dagger, \tag{G4}$$

where $\hat{\sigma} = \hat{T}(\hat{\rho} \otimes \hat{\pi}_e)\hat{T}^\dagger$, where we used $\hat{\pi}_e = \hat{U}_{g,e}\hat{\pi}_e\hat{U}_{g,e}^\dagger$. Hence,

$$\mathcal{E}[\hat{U}_{g,s}\hat{\rho}\hat{U}_{g,s}^\dagger] = \mathrm{Tr}_e[\hat{U}_{g,s} \otimes \hat{U}_{g,e}(\hat{\sigma})\hat{U}_{g,s}^\dagger \otimes \hat{U}_{g,e}^\dagger]. \tag{G5}$$

Since the partial trace over the environment commutes with unitaries on the environment, one gets

$$\begin{aligned}\mathrm{Tr}_e[\hat{U}_{g,s} \otimes \hat{U}_{g,e}(\hat{\sigma})\hat{U}_{g,s}^\dagger \otimes \hat{U}_{g,e}^\dagger] &= \hat{U}_{g,s}\mathrm{Tr}_e[\hat{\sigma}]\hat{U}_{g,s}^\dagger \\ &= \hat{U}_{g,s}\mathcal{E}[\hat{\rho}]\hat{U}_{g,s}^\dagger.\end{aligned} \tag{G6}$$

Thus,

$$\mathcal{E}[\hat{U}_{g,s}\hat{\rho}\hat{U}_{g,s}^\dagger] = \hat{U}_{g,s}\mathcal{E}[\hat{\rho}]U_{g,s}^\dagger, \tag{G7}$$

showing that $\mathcal{E}$ is G-covariant whenever $\hat{U}$ is G-invariant and $\hat{\pi}$ is G-invariant.

[1] E. B. Mpemba and D. G. Osborne, *Cool?*, Phys. Educ. **4**, 172 (1969).
[2] Yun-Ho Ahn, Hyery Kang, Dong-Yeun Koh, and Huen Lee, *Experimental verifications of Mpemba-like behaviors of clathrate hydrates*, Korean J. Chem. Eng. **33**, 1903 (2016).

[3] Cunliang Hu, Jingqing Li, Shaoyong Huang, Hongfei Li, Chuanfu Luo, Jizhong Chen, Shichun Jiang, and Lijia An, *Conformation directed Mpemba effect on polylactide crystallization*, Cryst. Growth Des. **18**, 5757 (2018).

[4] P. Chaddah, S. Dash, Kranti Kumar, and A. Banerjee, *Overtaking while approaching equilibrium*, arXiv:1011.3598.

[5] Zhiyue Lu and Oren Raz, *Nonequilibrium thermodynamics of the Markovian Mpemba effect and its inverse*, Proc. Natl. Acad. Sci. U.S.A. **114**, 5083 (2017).

[6] Israel Klich, Oren Raz, Ori Hirschberg, and Marija Vucelja, *Mpemba index and anomalous relaxation*, Phys. Rev. X **9**, 021060 (2019).

[7] A. Gal and O. Raz, *Precooling strategy allows exponentially faster heating*, Phys. Rev. Lett. **124**, 060602 (2020).

[8] Gianluca Teza, Ran Yaacoby, and Oren Raz, *Relaxation shortcuts through boundary coupling*, Phys. Rev. Lett. **131**, 017101 (2023).

[9] Gianluca Teza, John Bechhoefer, Antonio Lasanta, Oren Raz, and Marija Vucelja, *Speedups in nonequilibrium thermal relaxation: Mpemba and related effects*, Phys. Rep. **1164**, 1 (2026).

[10] Avinash Kumar and John Bechhoefer, *Exponentially faster cooling in a colloidal system*, Nature (London) **584**, 64 (2020).

[11] Avinash Kumar, Raphaël Chétrite, and John Bechhoefer, *Anomalous heating in a colloidal system*, Proc. Natl. Acad. Sci. U.S.A. **119**, e2118484119 (2022).

[12] Isha Malhotra and Hartmut Löwen, *Double Mpemba effect in the cooling of trapped colloids*, arXiv:2406.19098.

[13] A. Lasanta, F. Vega Reyes, A. Prados, and A. Santos, *When the hotter cools more quickly: Mpemba effect in granular fluids*, Phys. Rev. Lett. **119**, 148001 (2017).

[14] Apurba Biswas, V. V. Prasad, O. Raz, and R. Rajesh, *Mpemba effect in driven granular Maxwell gases*, Phys. Rev. E **102**, 012906 (2020).

[15] Zhen-Yu Yang and Ji-Xuan Hou, *Non-Markovian Mpemba effect in mean-field systems*, Phys. Rev. E **101**, 052106 (2020).

[16] Sheng Zhang and Ji-Xuan Hou, *Theoretical model for the Mpemba effect through the canonical first-order phase transition*, Phys. Rev. E **106**, 034131 (2022).

[17] Monwhea Jeng, *The Mpemba effect: When can hot water freeze faster than cold?*, Am. J. Phys. **74**, 514 (2006).

[18] Henry C. Buridge and Oscar Hallstadius, *Observing the Mpemba effect with minimal bias and the value of the Mpemba effect to scientific outreach and engagement*, Proc. R. Soc. A **476**, 20190829 (2020).

[19] Andrea Nava and Michele Fabrizio, *Lindblad dissipative dynamics in the presence of phase coexistence*, Phys. Rev. B **100**, 125102 (2019).

[20] Federico Carollo, Antonio Lasanta, and Igor Lesanovsky, *Exponentially accelerated approach to stationarity in markovian open quantum systems through the Mpemba effect*, Phys. Rev. Lett. **127**, 060401 (2021).

[21] Ruicheng Bao and Zhonghuai Hou, *Accelerating relaxation in Markovian open quantum systems through quantum reset processes*, Phys. Rev. Lett. **135**, 150403 (2025).

[22] Simon Kochsiek, Federico Carollo, and Igor Lesanovsky, *Accelerating the approach of dissipative quantum spin systems towards stationarity through global spin rotations*, Phys. Rev. A **106**, 012207 (2022).

[23] Felix Ivander, Nicholas Anto-Sztrikacs, and Dvira Segal, *Hyperacceleration of quantum thermalization dynamics by bypassing long-lived coherences: An analytical treatment*, Phys. Rev. E **108**, 014130 (2023).

[24] Xuanhua Wang and Jin Wang, *Mpemba effects in nonequilibrium open quantum systems*, Phys. Rev. Res. **6**, 033330 (2024).

[25] S. Aharony Shapira, Y. Shapira, J. Markov, G. Teza, N. Akerman, O. Raz, and R. Ozeri, *Inverse Mpemba effect demonstrated on a single trapped ion qubit*, Phys. Rev. Lett. **133**, 010403 (2024).

[26] Mattia Moroder, Oisín Culhane, Krissia Zawadzki, and John Goold, *Thermodynamics of the quantum Mpemba effect*, Phys. Rev. Lett. **133**, 140404 (2024).

[27] David J. Strachan, Archak Purkayastha, and Stephen R. Clark, *Non-Markovian quantum Mpemba effect*, Phys. Rev. Lett. **134**, 220403 (2025).

[28] Ivan Medina, Oisín Culhane, Felix C. Binder, Gabriel T. Landi, and John Goold, *Anomalous discharging of quantum batteries: The ergotropic Mpemba effect*, Phys. Rev. Lett. **134**, 220402 (2025).

[29] Mingdi Xu, Zijun Wei, Xiang-Ping Jiang, and Lei Pan, *Expedited thermalization dynamics in incommensurate systems*, Phys. Rev. A **112**, 042210 (2025).

[30] Philipp Westhoff, Sebastian Paeckel, and Mattia Moroder, *Fast and direct preparation of a genuine lattice Bose-Einstein condensate via the quantum Mpemba effect*, Phys. Rev. A **112**, 061304 (2025).

[31] N. Beato and G. Teza, *Relaxation control of open quantum systems*, Phys. Rev. Lett. **136**, 070401 (2026).

[32] Throughout this paper, we consider dynamics on a composite Hilbert space $\mathscr{H} = \mathscr{H}_s \otimes \mathscr{H}_e$, where $\mathscr{H}_s$ (system) and $\mathscr{H}_e$ (environment) are always distinguished. In the open-dynamics case, $\mathscr{H}_e$ describes an external bath; in the closed-dynamics case, $\mathscr{H}_e$ is the complementary subsystem within an overall isolated $\mathscr{H}$. *Local* symmetry restoration then means that, after evolving under the joint dynamics, we apply the partial trace Tr_e and study symmetry recovery on the reduced state $\hat{\rho}_s = \mathrm{Tr}_e[\hat{\sigma}]$.

[33] Filiberto Ares, Sara Murciano, and Pasquale Calabrese, *Entanglement asymmetry as a probe of symmetry breaking*, Nat. Commun. **14**, 2036 (2023).

[34] Filiberto Ares, Pasquale Calabrese, and Sara Murciano, *The quantum Mpemba effects*, Nat. Rev. Phys. (2025), 10.1038/s42254-025-00838-0.

[35] Bob Coecke, Tobias Fritz, and Robert W. Spekkens, *A mathematical theory of resources*, Inf. Comput. **250**, 59 (2016).

[36] Eric Chitambar and Gilad Gour, *Quantum resource theories*, Rev. Mod. Phys. **91**, 025001 (2019).

[37] Iman Marvian and Robert W. Spekkens, *Modes of asymmetry: The application of harmonic analysis to symmetric quantum dynamics and quantum reference frames*, Phys. Rev. A **90**, 062110 (2014).

[38] John Goold, Marcus Huber, Arnau Riera, Lídia del Rio, and Paul Skrzypczyk, *The role of quantum information in thermodynamics—A topical review*, J. Phys. A **49**, 143001 (2016).

[39] We indicate by $\mathscr{S}(\mathscr{H}_s)$ the set of density matrices on $\mathscr{H}_s$.

[40] R. Horodecki, P. Horodecki, M. Horodecki, and K. Horodecki, *Quantum entanglement*, Rev. Mod. Phys. **81**, 865 (2009).

[41] Philippe Faist, Jonathan Oppenheim, and Renato Renner, *Gibbs-preserving maps outperform thermal operations in the quantum regime*, New J. Phys. **17**, 043003 (2015).

[42] Milán Mosonyi and Fumio Hiai, *On the quantum Rényi relative entropies and related capacity formulas*, IEEE Trans. Inf. Theory **57**, 2474 (2011).

[43] Gilad Gour and Robert W. Spekkens, *The resource theory of quantum reference frames: Manipulations and monotones*, New J. Phys. **10**, 033023 (2008).

[44] Matthew J. Donald, *Free energy and the relative entropy*, J. Stat. Phys. **49**, 81 (1987).

[45] F. G. S. L. Brandão, M. Horodecki, J. Oppenheim, J. M. Renes, and R. W. Spekkens, *Resource theory of quantum states out of thermal equilibrium*, Phys. Rev. Lett. **111**, 250404 (2013).

[46] Matteo Lostaglio, David Jennings, and Terry Rudolph, *Description of quantum coherence in thermodynamic processes requires constraints beyond free energy*, Nat. Commun. **6**, 6383 (2015).

[47] Massimiliano Esposito, Katja Lindenberg, and Christian Van den Broeck, *Entropy production as correlation between system and reservoir*, New J. Phys. **12**, 013013 (2010).

[48] Udo Seifert, *Stochastic thermodynamics, fluctuation theorems and molecular machines*, Rep. Prog. Phys. **75**, 126001 (2012).

[49] Matteo Lostaglio, *An introductory review of the resource theory approach to thermodynamics*, Rep. Prog. Phys. **82**, 114001 (2019).

[50] David J. C. MacKay, *Information Theory, Inference & Learning Algorithms* (Cambridge University Press, Cambridge, England, 2002).

[51] Nelly Huei Ying Ng and Mischa Prebin Woods, *Resource theory of quantum thermodynamics: Thermal operations and second laws*, in *Thermodynamics in the Quantum Regime: Fundamental Aspects and New Directions*, edited by Felix Binder, Luis A. Correa, Christian Gogolin, Janet Anders, and Gerardo Adesso (Springer International Publishing, Cham, 2018), pp. 625–650.

[52] Tan Van Vu and Hisao Hayakawa, *Thermomajorization Mpemba effect*, Phys. Rev. Lett. **134**, 107101 (2025).

[53] Andrea Nava and Reinhold Egger, *Mpemba effects in open nonequilibrium quantum systems*, Phys. Rev. Lett. **133**, 136302 (2024).

[54] Doruk Can Alyürük, Mahir H. Yeşiller, Vlatko Vedral, and Onur Pusuluk, *Thermodynamic limits of the Mpemba effect: A unified resource theory analysis*, arXiv:2502.00123.

[55] Gianluca Teza, Ran Yaacoby, and Oren Raz, *Eigenvalue crossing as a phase transition in relaxation dynamics*, Phys. Rev. Lett. **130**, 207103 (2023).

[56] Michael Manhart, *Markov Processes*, Lecture Notes for Physics Vol. 677 (Rutgers University, 2016), https://www.physics.rutgers.edu/morozov/677-f2016/Physics-677-2016-files/Manhart-Markov-Processes–2016.pdf.

[57] A. Libál, C. Nisoli, and C. J. Olson Reichhardt, *Dynamic control of topological defects in artificial colloidal ice*, Sci. Rep. **7**, 651 (2017).

[58] Marco Tomamichel, *Quantum Information Processing with Finite Resources* (Springer International, New York, 2016).

[59] E. B. Davies, *Generators of dynamical semigroups*, J. Funct. Anal. **34**, 421 (1979).

[60] Matteo Lostaglio, Álvaro M. Alhambra, and Christopher Perry, *Elementary thermal operations*, Quantum **2**, 52 (2018).

[61] Robert Alicki, *On the detailed balance condition for non-Hamiltonian systems*, Rep. Math. Phys. **10**, 249 (1976).

[62] Robert Alicki and Karl Lendi, *Quantum Dynamical Semigroups and Applications*, Lecture Notes in Physics Vol. 717 (Springer Berlin Heidelberg, Berlin, Heidelberg, 2007), 10.1007/3-540-70861-8.

[63] Dongheng Qian, Huan Wang, and Jing Wang, *Intrinsic quantum Mpemba effect in Markovian systems and quantum circuits*, arXiv:2411.18417.

[64] Dénes Petz, *Monotone metrics on matrix spaces*, Linear Algebra Appl. **244**, 81 (1996).

[65] Georgios Styliaris and Paolo Zanardi, *Symmetries and monotones in Markovian quantum dynamics*, Quantum **4**, 261 (2020).

[66] Matteo Scandi, Paolo Abiuso, Jacopo Surace, and Dario De Santis, *Quantum Fisher information and its dynamical nature*, Rep. Prog. Phys. **88**, 076001 (2025).

[67] Iman Marvian and Robert W. Spekkens, *Extending Noether's theorem by quantifying the asymmetry of quantum states*, Nat. Commun. **5**, 3821 (2014).

[68] Colin Rylands, Katja Klobas, Filiberto Ares, Pasquale Calabrese, Sara Murciano, and Bruno Bertini, *Microscopic origin of the quantum Mpemba effect in integrable systems*, Phys. Rev. Lett. **133**, 010401 (2024).

[69] Sara Murciano, Filiberto Ares, Israel Klich, and Pasquale Calabrese, *Entanglement asymmetry and quantum Mpemba effect in the XY spin chain*, J. Stat. Mech. (2024) 013103.

[70] Giuseppe Di Giulio, Xhek Turkeshi, and Sara Murciano, *Measurement-induced symmetry restoration and quantum Mpemba effect*, Entropy **27**, 407 (2025).

[71] Shion Yamashika, Filiberto Ares, and Pasquale Calabrese, *Entanglement asymmetry and quantum Mpemba effect in two-dimensional free-fermion systems*, Phys. Rev. B **110**, 085126 (2024).

[72] X. Turkeshi, P. Calabrese, and A. De Luca, *Quantum Mpemba effect in random circuits*, Phys. Rev. Lett. **135**, 040403 (2025).

[73] Shuo Liu, Hao-Kai Zhang, Shuai Yin, and Shi-Xin Zhang, *Symmetry restoration and quantum Mpemba effect in symmetric random circuits*, Phys. Rev. Lett. **133**, 140405 (2024).

[74] Filiberto Ares, Sara Murciano, Pasquale Calabrese, and Lorenzo Piroli, *Entanglement asymmetry dynamics in random quantum circuits*, Phys. Rev. Res. **7**, 033135 (2025).

[75] Lata Kh. Joshi, Johannes Franke, Aniket Rath, Filiberto Ares, Sara Murciano, Florian Kranzl, Rainer Blatt, Peter Zoller, Benoît Vermersch, Pasquale Calabrese, Christian F. Roos, and Manoj K. Joshi, *Observing the quantum Mpemba effect in quantum simulations*, Phys. Rev. Lett. **133**, 010402 (2024).

[76] Noether's first theorem originally applied to continuous (Lie) groups of differentiable symmetries, but its principles have since been extended to include discrete symmetries such as parity or time reversal.

[77] Yvette Kosmann-Schwarzbach and Bertram E. Schwarzbach, *The Noether Theorems: Invariance and Conservation Laws in the Twentieth Century* (Springer, New York, 2011).

[78] E. Noether, *Invariante variationsprobleme*, Nachr. Ges. Wiss. Gött. Math.-Phys. Klasse **1918**, 235 (1918), https://eudml.org/doc/59024.

[79] Victor V. Albert and Liang Jiang, *Symmetries and conserved quantities in Lindblad master equations*, Phys. Rev. A **89**, 022118 (2014).

[80] Physically, the more relevant property is that the ratios of Bohr frequencies $E_i - E_j$ are rational numbers, in which case the corresponding unitary group forms a projective representation of U(1).

[81] Katja Klobas, Colin Rylands, and Bruno Bertini, *Translation symmetry restoration under random unitary dynamics*, Phys. Rev. B **111**, L140304 (2025).

[82] Florent Ferro, Filiberto Ares, and Pasquale Calabrese, *Non-equilibrium entanglement asymmetry for discrete groups: The example of the xy spin chain*, J. Stat. Mech. (2024) 023101.

[83] Berislav Buča and Tomaž Prosen, *A note on symmetry reductions of the Lindblad equation: Transport in constrained open spin chains*, New J. Phys. **14**, 073007 (2012).

[84] M. Keyl and R. F. Werner, *Optimal cloning of pure states, testing single clones*, J. Math. Phys. (N.Y.) **40**, 3283 (1999).

[85] Iman Marvian, *Symmetry, asymmetry and quantum information*, Ph.D. thesis, University of Waterloo, https://uwspace.uwaterloo.ca/handle/10012/7088 (2012).

[86] This is sometimes known as the covariant Stinespring dilation theorem.

[87] A broad class of maps that are guaranteed to restore a symmetry consists of quantum Markov processes with a fixed point, as shown in Ref. [88]. However, non-Markovian examples also exist, such as spin star systems [89].

[88] Alberto Frigerio, *Stationary states of quantum dynamical semigroups*, Commun. Math. Phys. **63**, 269 (1978).

[89] Heinz-Peter Breuer, Daniel Burgarth, and Francesco Petruccione, *Non-markovian dynamics in a spin star system: Exact solution and approximation techniques*, Phys. Rev. B **70**, 045323 (2004).

[90] Iman Marvian and Robert W. Spekkens, *How to quantify coherence: Distinguishing speakable and unspeakable notions*, Phys. Rev. A **94**, 052324 (2016).

[91] For channels with multiple Kraus operators, the requirement of G invariance [Eq. (25)] must hold for each Kraus element individually. Equivalently, one can demand that the Lindblad generator be unchanged under independent left- and right-unitary twists, $\mathcal{U}_g^{(L)}\mathcal{L}\mathcal{U}_g^{(L)\dagger} = \mathcal{U}_g^{(R)}\mathcal{L}\mathcal{U}_g^{(R)\dagger} = \mathcal{L} \quad \forall\ g \in \mathrm{G}$, where $\mathcal{U}_g^{(L)}[\hat{\rho}] = \hat{U}_g\hat{\rho}$ (ket action) and $\mathcal{U}_g^{(R)}[\hat{\rho}] = \hat{\rho}\hat{U}_g^\dagger$ (bra action) [79,83].

[92] Dominik Janzing, *Quantum thermodynamics with missing reference frames: Decompositions of free energy into non-increasing components*, J. Stat. Phys. **125**, 761 (2006).

[93] Stephen D. Bartlett, Terry Rudolph, and Robert W. Spekkens, *Reference frames, superselection rules, and quantum information*, Rev. Mod. Phys. **79**, 555 (2007).

[94] Iman Marvian and Robert W. Spekkens, *The theory of manipulations of pure state asymmetry: I. Basic tools, equivalence classes and single copy transformations*, New J. Phys. **15**, 033001 (2013).

[95] Gilad Gour, Iman Marvian, and Robert W. Spekkens, *Measuring the quality of a quantum reference frame: The relative entropy of frameness*, Phys. Rev. A **80**, 012307 (2009).

[96] J. A. Vaccaro, F. Anselmi, H. M. Wiseman, and K. Jacobs, *Tradeoff between extractable mechanical work, accessible entanglement, and ability to act as a reference system, under arbitrary superselection rules*, Phys. Rev. A **77**, 032114 (2008).

[97] In the case of equal real parts, modes are further ordered by increasing μ and then by decreasing the imaginary part.

[98] Iman Marvian, *Restrictions on realizable unitary operations imposed by symmetry and locality*, Nat. Phys. **18**, 283 (2022).

[99] Iman Marvian, *Theory of quantum circuits with Abelian symmetries*, Phys. Rev. Res. **6**, 043292 (2024).

[100] Alessandro Summer, Alex Nico-Katz, Shane Dooley, and John Goold, *Anomalous transport in U(1)-symmetric quantum circuits*, arXiv:2411.14357.

[101] D. Burgarth, G. Chiribella, V. Giovannetti, P. Perinotti, and K. Yuasa, *Ergodic and mixing quantum channels in finite dimensions*, New J. Phys. **15**, 073045 (2013).

[102] Heinz-Peter Breuer, Elsi-Mari Laine, Jyrki Piilo, and Bassano Vacchini, *Colloquium: Non-Markovian dynamics in open quantum systems*, Rev. Mod. Phys. **88**, 021002 (2016).

[103] Rui-An Chang, Harshank Shrotriya, Wen Wei Ho, and Matteo Ippoliti, *Deep thermalization under charge-conserving quantum dynamics*, PRX Quantum **6**, 020343 (2025).

[104] Kristian Wold, Zitian Zhu, Feitong Jin, Xuhao Zhu, Zehang Bao, Jiarun Zhong, Fanhao Shen, Pengfei Zhang, Hekang Li, Zhen Wang, Chao Song, Qiujiang Guo, Sergey Denisov, Lucas Sá, H. Wang, and Pedro Ribeiro, *Experimental detection of dissipative quantum chaos*, arXiv:2506.04325.

[105] Jader P. Santos, Lucas C. Céleri, Gabriel T. Landi, and Mauro Paternostro, *The role of quantum coherence in non-equilibrium entropy production*, npj Quantum Inf. **5** (2019).

[106] The resource theory of symmetry-respecting athermality is defined by the free states $\mathscr{F} = \{\hat{\rho}|\mathcal{G}[\hat{\rho}] = \hat{\pi}\}$ and the free operations given by G-covariant TOs, such as the Davies map in our example. By construction, any free operation $\mathcal{E}$ maps free states to free states: G covariance, $\mathcal{U}_g \circ \mathcal{E} = \mathcal{E} \circ \mathcal{U}_g$, implies $\mathcal{G} \circ \mathcal{E} = \mathcal{E} \circ \mathcal{G}$, so for $\hat{\rho} \in \mathscr{F}$ one has $\mathcal{G}[\mathcal{E}[\hat{\rho}]] = \mathcal{E}[\mathcal{G}[\hat{\rho}]] = \mathcal{E}[\hat{\pi}] = \hat{\pi}$, and, hence, $\mathcal{E}[\hat{\rho}] \in \mathscr{F}$.

[107] A. Summer, M. Moroder, and L. P. Bettmann, resource_-theory_mpemba, https://github.com/alessum/resource_theory_mpemba.

[108] G. Manzano, J. M. Horowitz, and Juan M. R. Parrondo, *Quantum fluctuation theorems for arbitrary environments:*

Adiabatic and nonadiabatic entropy production, Phys. Rev. X **8**, 031037 (2018).

[109] Herbert Spohn, *Entropy production for quantum dynamical semigroups*, J. Math. Phys. (N.Y.) **19**, 1227 (1978).

[110] Immanuel Bloch, Jean Dalibard, and Wilhelm Zwerger, *Many-body physics with ultracold gases*, Rev. Mod. Phys. **80**, 885 (2008).

[111] Tony E. Lee, H. Häffner, and M. C. Cross, *Collective quantum jumps of Rydberg atoms*, Phys. Rev. Lett. **108**, 023602 (2012).

[112] Augustine Kshetrimayum, Hendrik Weimer, and Román Orús, *A simple tensor network algorithm for two-dimensional steady states*, Nat. Commun. **8**, 1291 (2017).

[113] Tanmay Bhore, Lei Su, Ivar Martin, Aashish A. Clerk, and Zlatko Papić, *Quantum Mpemba effect without global symmetries*, Phys. Rev. B **112**, L121109 (2025).

[114] Mark Srednicki, *Chaos and quantum thermalization*, Phys. Rev. E **50**, 888 (1994).

[115] J. M. Deutsch, *Quantum statistical mechanics in a closed system*, Phys. Rev. A **43**, 2046 (1991).

[116] Peter O'Donovan, Philipp Strasberg, Kavan Modi, John Goold, and Mark T. Mitchison, *Quantum master equation from the eigenstate thermalization hypothesis*, Phys. Rev. B **112**, 014312 (2025).

[117] Matteo Lostaglio, Kamil Korzekwa, and Antony Milne, *Markovian evolution of quantum coherence under symmetric dynamics*, Phys. Rev. A **96**, 032109 (2017).

[118] Matteo Polettini and Massimiliano Esposito, *Nonconvexity of the relative entropy for Markov dynamics: A Fisher information approach*, Phys. Rev. E **88**, 012112 (2013).

[119] Yu Cao, Jianfeng Lu, and Yulong Lu, *Gradient flow structure and exponential decay of the sandwiched Rényi divergence for primitive lindblad equations with GNS-detailed balance*, J. Math. Phys. (N.Y.) **60**, 052202 (2019).